Comparative Characteristics of Seismic and Deformation Effects for Three Great Subduction Megaearthquakes

A. A. Lukk[a], * and V. G. Leonova[a]

[a]Schmidt Institute of Physics of the Earth, Russian Academy of Sciences, Moscow, 123242 Russia
**e-mail: lukk@ifz.ru*

Abstract—The comparative characteristics of seismic and deformational effects of three great subduction megaearthquakes in Sumatra in 2004 ($M_w = 9.2$); in Maule, Chile, in 2010 ($M_w = 8.8$); and in Tohoku, Japan, in 2011 ($M_w = 9.0$) are considered. In all cases the main rupture at the time of the earthquake was located in the subduction zone on the surface of the oceanic lithospheric plate plunging gently beneath a continent or an island arc. The process of destruction in each focus is characterized by a megathrust, with a gentle inclination angle of $\sim 8-18°$, according to the definitions of its focal mechanism, in almost full compliance with a gentle dipping of the oceanic lithospheric plate. The displacement occurred in a locked area of the subducting plate extended for several kilometers below the ocean bottom to a depth of 30–40 km. In all three cases, the maximum coseismic slip, obtained according to the data of geodetic measurements, occurred in the upper 25 km of the locked area, while its lower part radiated coherent short-period seisms. The trace of the rupture on the surface, marked by the aftershock area, ranged from 400–600 km in the case of Tohoku and Maule earthquakes up to ~1500 km during the Sumatra earthquake. The rupture in the Maule and Tohoku earthquakes was bilateral, with its approximately symmetric propagation from the epicenter, while in the Sumatra earthquake the rupture spread unilaterally relative to the epicenter from southeast to northwest. The propagation time of the rupture also varied. If in the first two cases it was 140–160 s, for the Sumatra earthquake it lasted 500–600 s. The largest tsunami wave, up to 40–60 m in height, was recorded during the Tohoku earthquake, extending for more than 200 km along the coast of Sanriku province. The rupture during the megaearthquakes under discussion is not confined in depth to the locked seismogenic area, marked by the area of the aftershock nearest in time and the zone of maximum coseismic slips determined by the geodetic GPS measurements. The rupture continues aseismically (postseismic slip) in the transition zone from brittle to brittle-plastic slip to depths of ~60–80 km. In addition, there is evidence that the displacements on the megathrust can continue slightly deeper to the region of the brittle–plastic slip. Such episodic events of slow slip ("silent" or "slow" earthquakes) and "seismic tremor" were recorded in southwestern Japan and southern Chile. These differences in seismic and deformation effects can serve as evidence of the change in frictional properties with depth along the surface of the megathrust. It should also be recognized that the strength barriers and asperities on the megathrust surface expressed in certain geological structures or yet unclear nature of segments of high frequency radiation can manifest themselves in the character of distribution of the accompanying seismicity during the great subduction earthquakes.

Keywords: subduction, lithospheric plate, megathrust, earthquake, aftershocks, coseismic slip, strength barriers

DOI: 10.1134/S0001433820100060

INTRODUCTION

Five great subduction earthquakes with magnitudes of ~9 and even higher occurred during the instrumental observation period. They are the catastrophic events in Chile on May 22, 1960 ($M_w = 9.5$); in Alaska on March 28, 1964 ($M_w = 9.2$); in Sumatra Island (Indonesia) on December 26, 2004 ($M_w = 9.2$); in Central Chile (Maule) on February 27, 2010 ($M_w = 8.8$); and in Japan (Tohoku) on March 11, 2011 ($M_w = 9.0$). In all cases the main rupture at the earthquake moment was located in the subduction zone on the oceanic lithosphere surface, plunging gently beneath the continent and being assumedly "locked" for a long time before the main

shock occurred. This was indicated by the noticeable weakening of seismicity in the zone of a future strong earthquake, called a *seismic gap* in seismology. The first two events occurred at the initial stage of instrumental observations in the absence of sufficiently dense seismic networks; therefore, they could not be described in full. Nevertheless, it was stated in (Parkin, 1969; Plafker, 1969; Kanamori, 1970; Ben-Menahem, 1971; Kanamori and Cipar, 1974; Ruff and Kanamori, 1980; Khazaradze et al., 2002) that in both cases the faulting character was in fact related to an underthrust dipping gently below the continent.

However, the seismological, geodetic, and morphological characteristics of three subsequent seismic catastrophes (2004, 2010, and 2011) were described in detail in multiple published works. The list of reference presented here is far from being complete. Upon a review of the literature sources, we gained insight into comparative characteristics of seismic and deformation effects during these three great subduction megaearthquakes, which we present in this work.

Despite the fact that the evident moving tectonic force, leading ultimately to the appearance of similar seismic events, is a process of underthrusting of the oceanic lithosphere beneath the continental lithosphere and such great earthquakes should seemingly be called *megaunderthrusts*, they are defined by the term *megathrust* in the English language literature. And this is not abuse of terminology. It is tacitly accepted that, during such earthquakes, a hanging wing of the subduction zone can displace upward, which can be caused by the reaction of elastic recovery to long-term elastic deformation of the locked zone of cohesion between the upper and lower lithospheric plates during the process of underthrusting of the oceanic lithosphere in the subduction zone. Such recovery is actually observed in the process of geodetic survey immediately after the main shock (e.g., (Vigny et al., 2005, 2011; Banerjee et al., 2007; Ozawa et al., 2011; Aron et al., 2013; Wang et al., 2018; etc.)). Thereby, the use of the term "megathrust" for the discussed subduction megaearthquakes is not inappropriate, despite their obvious primary cause, i.e., underthrusting of the oceanic lithosphere beneath the continental lithosphere in the subduction zone.

Such earthquakes, associated with a slip on flat planes 150−300 km in width along the dip and ~500 to ~1500 km in length along the strike, turn out to be much larger than any earthquake with a source in the continental crust. This position suggests that the elastic energy accumulated during the long-term collision of the oceanic and continental lithospheric plates is occasionally released in the subduction zones in the form of seismic events with the maximum admissible magnitude on the Earth (M_w = 8.8−9.5).

Therefore, it is interesting to consider the common properties and differences in effects of seismotectonic strains caused by such catastrophic seismic events in their spacetime neighborhood.

REGIONS OF MEGATHRUST FORMATION DURING THREE GREAT SUBDUCTION EARTHQUAKES

Figure 1 presents the regions of megathrusts for the earthquakes considered. Despite the fact that all three seismic events occurred in the similar geotectonic setting—the subduction zone of lithospheric plates—they differ significantly in the slip character during the

earthquake and the subsequent release of the accumulated energy.

For example, during the Maule (Chile) and Tohoku (Japan) earthquakes, the slip in the source spread in two directions from the epicenter of the main shock, which lies approximately in the middle of the aftershock zone (Figs. 1b, 1c) and, during the Sumatra earthquake, it spread in one direction from the epicenter located on the extreme southeastern tip of the aftershock zone (Fig. 1a). During the first two events, the total length of the rupture along the strike was about 500 km (e.g., (Vigni et al., 2011; Wang et al., 2018) etc.), while, during the Sumatra earthquake, the length of the rupture reached from 1300 to 1500 km according to different estimates (e.g., (Lay et al., 2005; Chlieh et al., 2007; Engdahl et al., 2007) etc.). Thus, we observe two types of gigantic earthquakes: a rather compact type (the Maule and Tohoku earthquakes) and a very extensive type (the Sumatra earthquake), although the earthquake magnitudes did not differ significantly. The rupture area was calculated by the spatial distribution of the nearest aftershocks (from 2 months to half a year).

The earthquakes also contrast each other by the duration of the rupture: about 2.5−3 min for Maule and Tohoku (Lay and Kanamori, 2011; Simons et al., 2011; Koper et al., 2012) and about 9−10 min for Sumatra (Ishii et al., 2005; Lay and Kanamori, 2011). The durations of the rupture propagations reconstructed for these three events by the waveforms in the teleseismic zone by the method of backward inversion (Ishii et al., 2005; Simons et al., 2011; Koper et al., 2012; Zhang et al., 2012; etc.) are presented in the form of normalized peak amplitudes of waveforms in Fig. 2. Here, the average rupture velocities are estimated for the Sumatra, Maule, and Tohoku earthquakes at 2.5−2.8 (Ni et al., 2005; Ishii et al., 2005; Ammon et al., 2005; Engdahl et al., 2007), 2.1−3.1 (Koper et al., 2012; Vigny et al., 2011) and 0.9−2.1 km/s (Simons et al., 2011; Zhang et al., 2012), respectively. Figure 2d presents the corresponding functions of the seismic moment rate according to (Lay and Kanamori, 2011).

It follows from the data in Fig. 2 that the time functions of the source are similar in form and duration for the Maule and Tohoku earthquakes, although the maximum value for the seismic moment during the Tohoku earthquake was about two times greater than for the Maule earthquake. At the same time, the duration of the rupture propagation during the Sumatra earthquake was three times longer than for the Maule and Tohoku earthquakes, and the maximum value of the seismic moment was about two times less for this earthquake than for the Maule earthquake and about three times less than for the Tohoku earthquake. The data presented suggest that the rupture during the Tohoku earthquake was the sharpest among three events considered, while during the Sumatra earthquake it was relatively slow and lengthy. This was evi-
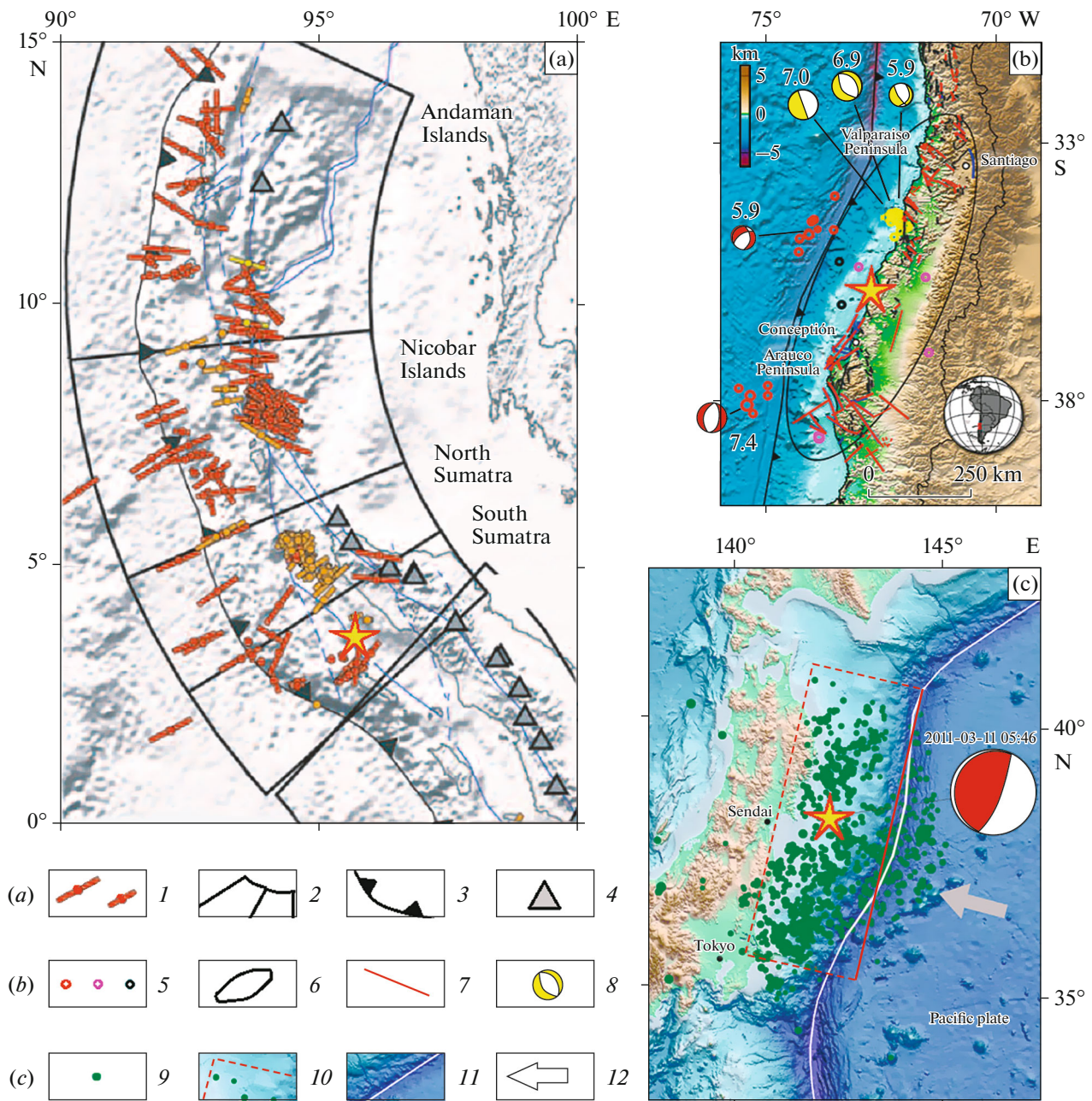
Fig. 1. Megathrust regions during three great subduction earthquakes: (a) Sumatra of 2004 (M_w = 9.2) (modified figure from (Engdahl et al., 2007. Fig. 9c)), (b) Chile (Maule) of 2010 (M_w = 8.8) (modified figure from (Aron et al., 2013. Fig. 1)), and (c) Japan (Tohoku) of 2011 (M_w = 9.0) (modified figure from (Zhang et al., 2012. Fig. 1)). (a) (1) Projections on the horizontal plane of tension axes T of all known CMT solutions for the aftershocks of the Sumatra earthquake nearest in time (December 26, 2004−March 27, 2005), (2) different segments of the megathrust plane, (3) oceanic trench axis in the vicinity of the Sunda arc (and in the coastal zone of central Chile), and (4) volcanoes; (b) (5) different groups of the Maule earthquake aftershocks for February 27, 2010−July 31, 2012, with a fault type of focal mechanisms untypical of a megathrust; (6) rupture region; (7) most vivid surface faults in the Earth's crust; and (8) particular examples of focal mechanism solutions with a fault type in the identified group of aftershocks; (c) (9) epicenters of the nearest aftershocks of the Tohoku earthquake (March 11, 2011−March 29, 2011), (10) approximate contours of the projection of the megathrust plane, (11) axis of the oceanic trench in the coastal zone of Japan, and (12) orientation of the Pacific Plate motion. The focal mechanism of the Tohoku earthquake is also shown.

denced in the significantly smaller values of released stresses in the greater part of the Sumatra rupture (they do not exceed 0.5 MPa) (Dewey et al., 2007) compared to the Maule (4.9 MPa according to (Aron et al., 2013)) and Tohoku (10 MPa, according to (Lay et al., 2012)) earthquakes. The complex character of the rupture during the Sumatra earthquake is also indicated by the necessity of adding to the calculations
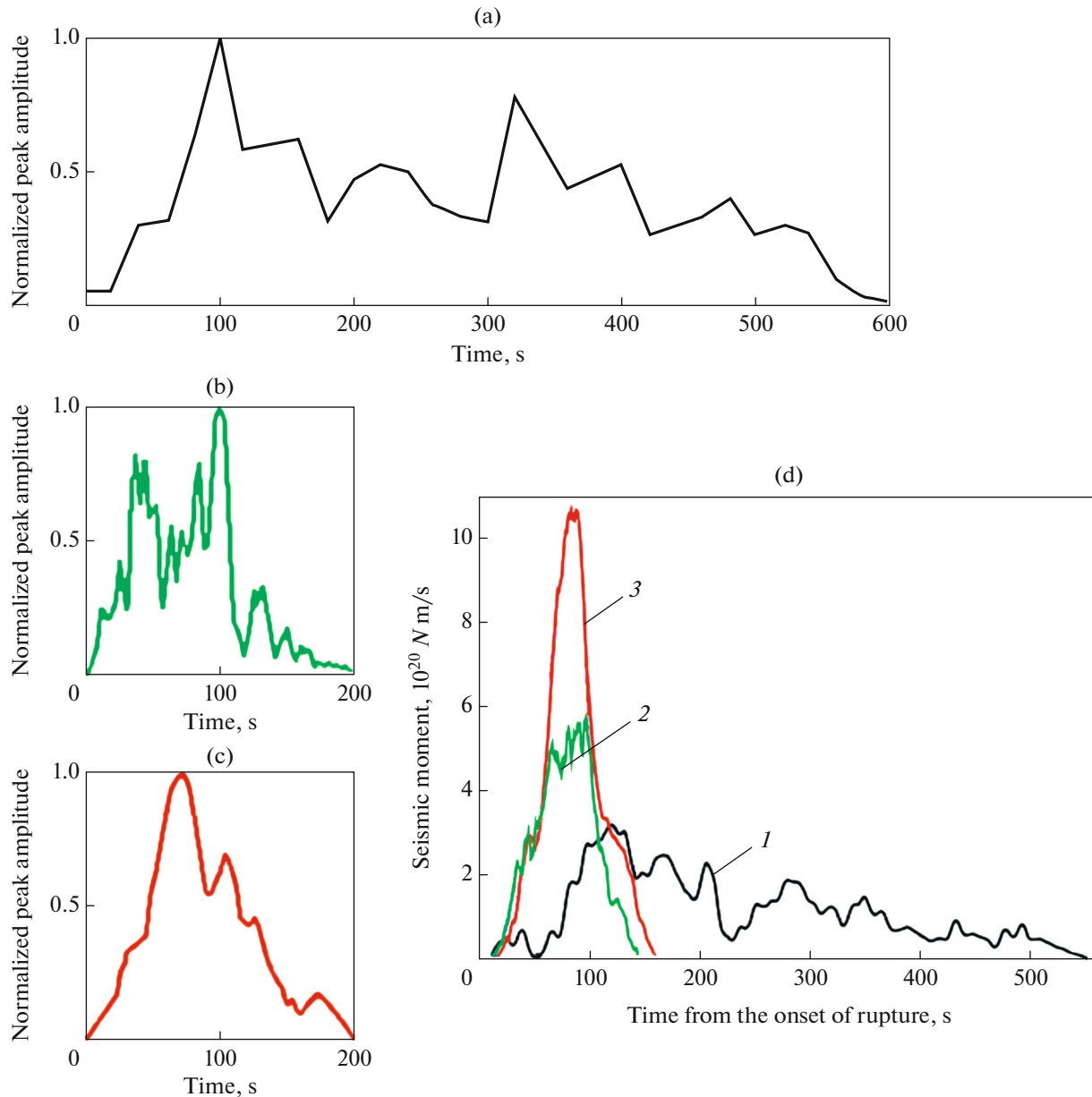
Fig. 2. Time functions of the source for (a) the Sumatra earthquake of 2004, $M_w = 9.2$ (modified figure from (Ishii et al., 2005, Fig. 3b)); (b) the Maule earthquake of 2010, $M_w = 8.8$ (modified figure from (Koper et al., 2012, Fig. 5a)); (c) the Tohoku earthquake of 2011, $M_w = 9.0$ (modified figure from (Simons et al., 2011)); and (d) corresponding functions of the seismic moment rate according to modified a figure from (Lay and Kanamori, 2011, Fig. 5). (d) (*1–3*) Earthquakes: (*1*) in Sumatra, (*2*) in Maule, (*3*) in Tohoku.

a variable velocity of its propagation from 2.8 km/s at the initial southeastern segment of the Sumatran fault to 2.0 km/s at its final northwestern segment (Guilbert et al., 2005; Chlieh et al., 2007; Engdahl et al., 2007).

One possible explanation for such marked differences of the rupturing process can be a different configuration in the displacement plane of the three seismic events being compared. The slip plane was straight along the strike for the Maule and Tohoku events, but its trace on the surface near the Sumatra earthquake

was curved (arc-wise). It changed orientation from northwestern at the southern tip of the rupture to meridional and even partly north-northeastern at the northern tip of the rupture. In addition, within the southern tip, the megathrust plane subducted at gentle angles (~12°–13°), but northward the inclination angle of the plane became steeper. These changes are vividly displayed in Fig. 3. Special estimates of these changes made in (Dewey et al., 2007) on the sectoral distribution of aftershocks with $mb \geq 5$ during the period of
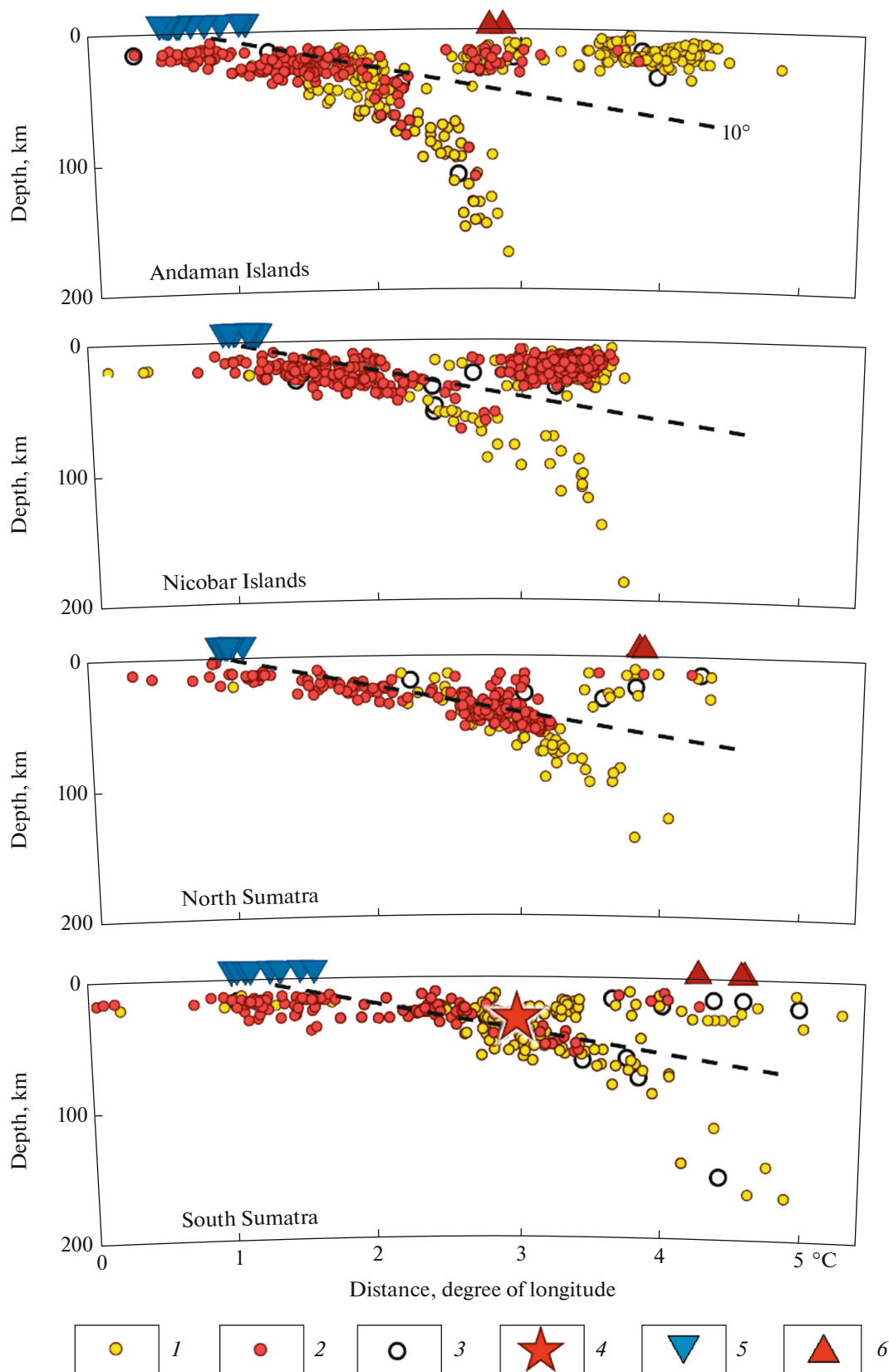
Fig. 3. Cross sections of clusters of earthquake hypocenters through the epicentral zone of aftershocks of the 2004 Sumatra earthquake with $M_w = 9.2$ for four sectors indicated in Fig. 1a (modified figure from (Shearer and Bungmann, 2010, Fig. 7); see also Fig. 6 in (Engdahl et al., 2007)). (*1*) Earthquakes before the main shock (January 1, 1964–December 26, 2004), (*2*) nearest in time aftershocks of the Sumatra earthquake (December 26, 2004–March 28, 2005), (*3*) early instrumental earthquakes (before 1964), (*4*) 2004 main shock hypocenter, (*5*) position of isolated points of the oceanic trench axis, and (*6*) volcanoes.

Table 1. Epicentral parameters and orientation of principal axes of focal mechanisms for three great subduction megaearthquakes (December 26, 2004–March 11, 2011)

Region	Catalog	Epicenter coordinates, deg	H, km	M_w	Principal axes of CMT and focal mechanism					
					P		T		B	
					Az, deg	α, deg	Az, deg	α, deg	Az, deg	α, deg
Sumatra	GCMT	03.09° N; 94.26° E	29		222	38	036	52	130	03
	NEIC	03.30° N; 95.98° E	30	9.2	213	34	050	55	308	08
	ISC	03.32° N; 95.98° E	27							
Maule	GCMT	35.98° S; 73.15° W	23		269	28	070	61	174	08
	NEIC	35.77° S; 72.47° W	30	8.8	272	26	080	63	180	04
	ISC	36.27° S; 72.91° W	23							
Tohoku	GCMT	37.52° N; 143.05° E	20		115	35	295	55	205	00
	NEIC	38.32° N; 142.97° E	24	9.0	110	30	295	59	201	02
	ISC	38.30° N; 142.50° E	20		093	38	304	48	196	16

December 26, 2004–September 30, 2005 showed that, during the transition from the southern to the northern sector, the inclination angle changed from 12°–13° to 19°–20° (Dewey et al., 2007, Fig. 12). Almost the same range of changes in the inclination of the megathrust plane (from 12° to 17.5°) in the same direction was also presented in (Chlieh et al., 2007, Table 1).

The indicated changes in the strike of the megathrust plane, related most likely to the change in the direction of the interplate motion from oblique to a rupture at its southern tip to near-parallel at its northern tip, as well as the assumed changes in the age of the subducting lithosphere (from 50 Ma at the southern tip of Sumatra coast to 90 Ma along the North Andaman trench, according to (Subarya et al., 2006)), can determine the character of slip during the Sumatra earthquake (Lay et al., 2005).

The width of the megathrust plane along its dip also changes along the strike, which is determined well by the width of the subducting zone of aftershocks of the Sumatra earthquake. It varies from ~200 km in the northern part of the rupture to ~275 km at its southern tip. In this case, the events located at a depth from 35 to 70 km are more often encountered in the southernmost part of this zone of aftershocks (Engdahl et al., 2007). The specific character of spatial location of aftershocks, their depths, and the occurrence of a total seismic moment in time led to the necessity of dividing the region of the Sumatra earthquake aftershocks into sectors accepted in (Engdahl et al., 2007) and shown in Fig. 1a.

In contrast to such a complex geometry of the rupture plane during the Sumatra earthquake and the related specific character of coseismic slip on this plane, the Maule and Tohoku earthquakes had much simpler geometry of the rupture plane and a relatively simple configuration of the coseismic slip on it. The Maule rupture propagated bilaterally from the epicenter, followed by the formation of two large patches of aftershock seismicity, having a similar size (Delouis et al., 2010; Tong et al., 2010; Lorito et al., 2011; Vigny et al., 2011; Lange et al., 2012), and the corresponding symmetrical patches of coseismic slip, up to 20 m in size in the northern patch and up to 10 m in the southern patch. The uniqueness of the Tohoku rupture was the high degree of aftershock concentration in the restricted area compared to the Sumatra earthquake, as well as the big (up to 60 m) values of slip on a relatively small portion of the fault extending for only ~300 km (typical for significantly weaker earthquakes with $M_w \approx 8.1$ according to (Wells and Coppersmith, 1994)), which sharply contrasts the length of the rupture zone of the Sumatra earthquake. This pulselike radiation of the Tohoku earthquake is well shown by the shape of the function of its seismic moment rate (Fig. 2d).

Of interest is the following circumstance. The regions of aftershocks end rather sharply at their northern and southern tips in all three events under consideration. This effect is generally related to the corresponding structural restrictions of the rupture propagation in the form of zones of tectonic dislocations transversal to its strike, rigid structural formations, or sharp changes in the strike of the tectonic zone where a seismogenic rupture occurred.

For example, Fig. 1c shows that the rupture zone of the Tohoku earthquake bumps with its southern tip into the northern boundary of the Philippine lithospheric plate, which is manifested well in the seafloor topography by the known Sagami trough (Ito et al., 2017), and, with its northern tip, into the southern boundary of the North American lithospheric plate, represented by the southern shelf of Hokkaido Island, which goes into a curvilinear junction of the South Kuril and Japan oceanic trenches.

Similar restrictions to the rupture propagation in the form of ruptures oblique to the main fault of the Earth's crust are also observed for the Maule earthquake (Fig. 1b). These ruptures are related primarily to the particular geological structures. For example, in the Pichilemu area, in the Huan-Fernandes ridge, there is an independent geological formation oblique to the main fault (Farías et al., 2011). The southern tip of the Maule rupture bumps into the Arauco Peninsula projecting into the Pacific Ocean—it is a large anomaly along the Pacific Ocean margin of South America in terms of costal morphology and the distance from the trench to the coast (Lin et al., 2013). The Arauco Peninsula is of special interest, because the boundary between the aftershock regions of the Maule earthquake and the great 1960 Chile earthquake with $M_w = 9.5$ go along it and, consequently, it can be considered a structural object of increased rigidity compared to its environment (Lin et al., 2013). There are ideas that the Earth's crust beneath the Arauco Peninsula is a zone of accumulation of shear strain on the faults oblique to the main fault and, therefore, it acts as a constant barrier for the propagation of seismic ruptures across it on a scale of millions of years (Barrientos and Ward, 1990; Melnick et al., 2009, 2012; Moreno et al., 2009; Delouis et al., 2010; Lay et al., 2010; Lin et al., 2013).

A similar situation was observed during the Sumatra earthquake in 2004. The southern tip of the rupture zone, where the earthquake epicenter was situated, bumped into Simeulue Island, located at the segment of a sudden change in the strike of the geologically identified Sumatran fault. This curve was likely a barrier between the epicentral areas of the 2004 Sumatra earthquake with $M_w = 9.2$ and the 2005 Nyasa earthquake with $M_w = 8.6$. The northern tip of the rupture ends near Preparas Island (~15° N) in the system of the Andaman Islands, where a complex geological cluster joining the Sumatran Fault and its extension the West Andaman fault, developing into the Sagaing Fault in the north, in Burma, is located. A rift center of expansion of the seafloor of the Andaman hollow is also found here. This last geostructural feature (the domination of the extension at the northern tip of the rupture) was likely to contribute to such a long length of the rupture during the Sumatra earthquake.

We also mention another typical feature. According to numerous messages, the epicentral zones of catastrophic megaearthquakes are often located between the two epicentral zones of the past catastrophic earthquakes. One gets the impression that, between these epicentral zones, there are rigid partitions that prevent the propagation of seismogenic ruptures during the catastrophic megaearthquakes. This, in turn, implies the possibility of segmentation of the subduction zones into separate elements (Lay et al., 2005; Dewey et al., 2007; Engdahl et al., 2007), which are activated separately from each other during seismic catastrophes. One of the variants of this segmentation scheme

is shown in Fig. 1a according to (Engdahl et al., 2007). The identical segmentation into two separate parts relative to the Maule earthquake epicenter is also indicated in (Melnick et al., 2009, 2012).

STRUCTURING OF SEISMIC EFFECTS ON THE MEGATHRUST SURFACE DURING THE GREAT SUBDUCTION EARTHQUAKES

Strong subduction earthquakes are generated in a restricted range of depths, usually from 20 to 50 km, rupturing a part of the plate interface, which is commonly called a seismogenic zone. These main interplate events are considered to generate in the part of the subducting plate surface that is fully or partly locked in a time interval between two successive seismic catastrophes within a seismic cycle (a locked zone in Fig. 4) and to rupture this part fully or partly; they can also spread deeper (Fig. 4) under the dynamics of the rupture process (e.g., (Scholz, 1998)). Estimating the width and a degree of blocking of the locked rupture zone (LRZ) is of primary importance for assessing a seismic hazard along subduction zones. This information can be extracted from the results of geodetic measurements of the interseismic deformation (e.g., (Oleskevich et al., 1999)).

The deformation character of the locked segment in the rupture zone can be traced by the example of the phenomenological model of the Tohoku earthquake considered in (Trubitsyn, 2011). The island plate in the subduction zone has been elastically deformed for several hundred years by convergence of the lithospheric plates. Its oceanic margin constantly descends and, near the island, a bending uplift appears. When the shear stress exceeds the cohesion force in the previously locked thrust zone, a slip occurs and this margin of the island plate is released; rises at 7—10 m; and thrusts over the oceanic plate, advancing towards the ocean at a distance to 20—30 m (Trubitsyn, 2011, p. 17).

The data on the rise of the island (upper) plate are of special importance, since the position of the maximum uplift value may serve as a good indicator of the projection onto the surface of the descending end of the LRZ (Fig. 4). The zone of the maximum vertical uplift of the upper plate surface is located nearly above the zone of transition to an aseismic slip at a depth. It is considered that earthquakes with magnitudes $M_w = 9.0$ originate along the LRZ, but the rupture may propagate further down to an aseismically slipping part of the plate interface. For simplicity, Fig. 4 does not show a transition zone between the fully locked part of the fault and the aseismic slip zone.

The current ideas on the seismic process in the subduction zone are that a part of the surface of the subducting plate (LRZ), which remains locked in the time interval between the largest earthquakes ($M_w = 9.0$) of one seismic cycle, does not spread to the mantle
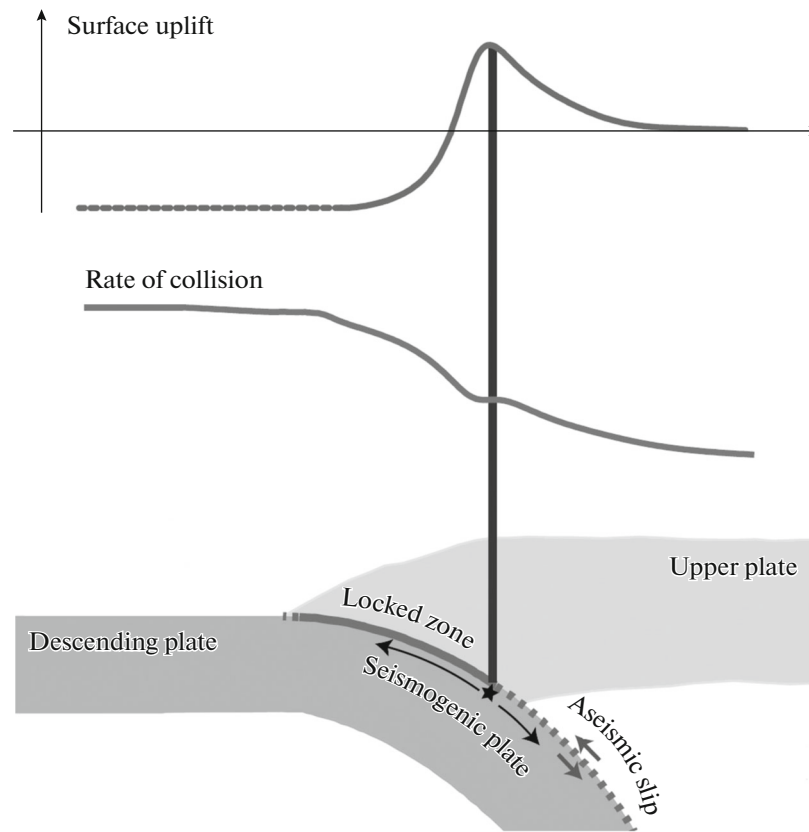
Fig. 4. Plot of the relationship among the geometry of the locked fault zone (LFZ), the value of the uplift of the upper plate, and the horizontal velocity of the subducting plate motion (modified figure from (Simoes et al., 2004, Fig. 1).

during the earthquake, since serpentinization of the mantle wedge contributes to a stable aseismic slip (Simoes et al., 2004). Nevertheless, studies on comparing the values of a horizontal displacement rate of the subducting oceanic plate obtained from GPS measurements of the horizontal deformation and the uplifts of the upper plate surface obtained from the long-term observations of the coral growth showed that the lower end of the LRZ sinks at a depth from 35 to 57 km, and the LRZ itself extends at ~130 km from the oceanic trench towards the island arc. By integrating this information and the geometry of the plate interface for the Sumatran collision zone determined from the seismicity distribution and the results of 2D gravimetric modeling, it was shown in (Simoes et al., 2004) that the LRZ propagates beneath the Moho boundary, which lies in the Sumatran subduction zone at a depth of ~30 km at a horizontal distance of ~110 km from the trench axis. In the same work, the temperature at the descending end of the LRZ is estimated at $260 \pm 100°C$. This temperature is too low for the thermally activated plastic flow; consequently, aseismic slip propagating further down to the LRZ is likely to occur as a stable brittle–plastic slip, whose parameters are determined by the pressure, temperature, and the presence of fluids at these depths.

The situation at the upper end of the LRZ is determined by the properties of the frontal part of the accretionary prism (a geological body formed during the subduction of the oceanic crust to the mantle in the subduction zone in the frontal part of the overlying continental plate) composed of soft sedimentary deposits that can deform without markedly expressed seismicity. The data on the growth of corals that are located close to the trench indicate a possible aseismic slip of the near-surface part of the thrust rupture (Natawidjaja et al., 2004). The position of this aseismic slip region on the megathrust earthquake plane for the Maule earthquake is shown in Fig. 5. Here, the base of the frontal part of the accretionary prism is marked by a dashed line designating the megathrust surface with an aseismic slip along it. The seismogenic zone that destroys the previously locked segment of the thrust fault zone is depicted in Fig. 5 as a region of coseismic slip. The seismogenic rupture that formed during the catastrophic earthquake is found exactly in this zone.

As a rule, the aftershocks nearest in time to the main rupture moment fill the previously locked region, where rather strong seismic events (less than the magnitude of the main shock by approximately two orders of magnitude), were absent for a long time
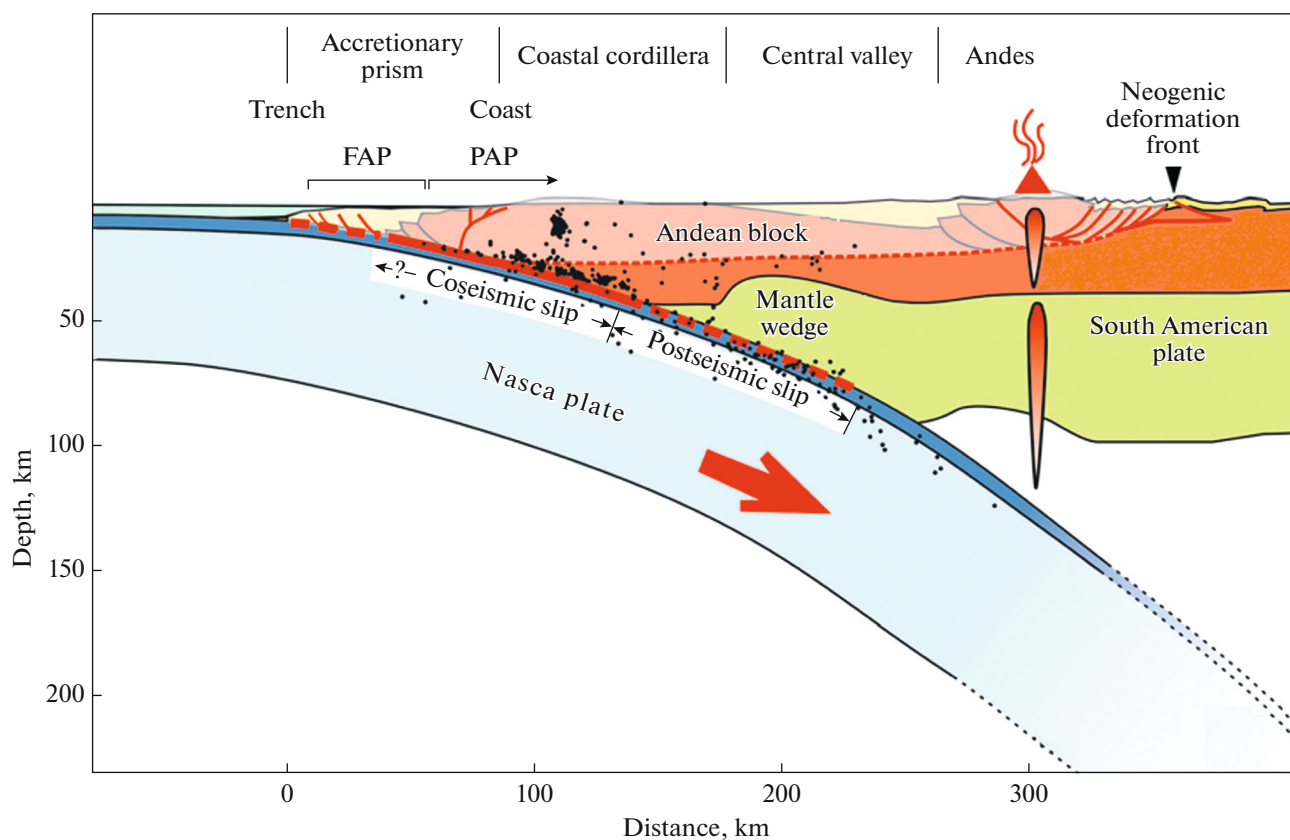
Fig. 5. Schematic cross section through the aftershock zone of the 2010 Maule earthquake (modified figure from (Lin et al., 2013, Fig. 1c)) FAP, frontal accretionary prism; PAP, paleoaccretionary prism. Dots designate background seismicity in November 2004−October 2005.

before the earthquake moment, thus forming a so-called seismic gap, which is widely used for the prediction of a future strong seismic event (Fedotov, 1968; Nersesov et al., 1976; Mogi, 1979; McCann et al., 1979; Nersesov and Rulev, 1986; Mogi, 1988; Kagan and Jackson, 1991; Lukk et al., 1996; Campos et al., 2002; etc.). In the case, with the catastrophic strong events described here, this effect was also partly recorded.

For example, during the Sumatra earthquake, the region of maximum slip on the rupture was located in the area that was almost free of earthquakes between the trench and the zone of high seismic activity in the period of 1964−2002 preceding the earthquake (Subarya et al., 2006, Fig. 3; Chlieh et al., 2007, Fig. 11). The epicenters of the aftershocks nearest in time to the main shock of the 2005 Sumatra earthquake (December 2004 to March 2005) lay at distances less than 35 km from the oceanic trench and filled the previously aseismic region (Engdahl et al., 2007, Fig. 4c).

The results of three campaigns of GPS measurements (1996, 1999, and 2002) performed on a network of 40 geodetic points in the south of central Chile indicated the existence of a zone of elastic strain accumulation (a region of seismic quiescence) in the epicen-

tral region of the future strong Maule earthquake in 2010 (Ruegg et al., 2009). The results of these measurements were interpreted as a fully coupled elastic load at an interface segment locked at a depth of ~55 km and at a distance of 180 km from the trench in the predicted megathrust plane with an inclination angle ~16° beneath the continent, where the displacement of >10 m is accumulated after the great earthquake of 1835 (Ruegg et al., 2009). To complete their description, the authors of the cited work stated that the southern part of the Concepción−Constitución rupture accumulated a slip deficit, which was large enough to trigger a very powerful earthquake with a magnitude of about $M_w = 8.0-8.5$ (Ruegg et al., 2009, p. 9)). The strong 2010 Maule earthquake, which occurred soon after the above work was published, filled the seismic gap (described in (McCann et al., 1979; Campos et al., 2002; Ruegg et al., 2009)) that showed only weak seismic activity after the previous catastrophic earthquake in 1835 (Lange et al., 2012). At the same time, it is suggested that the 2010 Maule earthquake with $M_w = 8.8$ turned out to be not strong enough to relax all elastic stresses that accumulated in this seismic gap, and there may still be the potential for a stronger event in the future (Moreno et al., 2010, 2011; Lorito et al., 2011; Lange et al., 2012).

The data of the geodetic measurements at some 400 points of GPS observations contributed to predicting the location of the 2011 Tohoku earthquake by constructing models that represent the future fault zone as a locked region on the surface of the plate subducting beneath the islands. (Tajima et al., 2013). In fact, the position of this locked segment seemed to be somewhat lower than the actual rupture zone in 2011. The rate of strain accumulation was much higher than the average rate of strain release from the previous interplate earthquakes (Tajima et al., 2013; Wang et al., 2018). However, it was properly assumed that an earthquake which should release the strain accumulated for several hundred years is going to occur in this region.

Of interest is the spatial comparison of the aftershock regions of the catastrophic earthquakes with the regions of coseismic and postseismic slip, which are identified by the data of GPS measurements. The regions of coseismic and postseismic slips tend to be located on different sides of the previous background seismicity (Chlieh et al., 2007; Ozawa et al., 2012; Lin et al., 2013). An example is shown in Fig. 6. Here, it is as if the region of preseismic slip separates the regions of coseismic and postseismic slips. The region of coseismic slip and the first aftershocks drive into the surface, accommodating themselves in the uppermost part of the megathrust at depths of 0−20 km (also Fig. 11 in (Chlieh et al., 2007)). It is noted that weak ($M_w < 4$) aftershocks are located in the regions with the highest level of coseismic slip, which is most likely related to the destruction processes in the region surrounding the megathrust plane (Agurto et al., 2012). At the same time, the strongest ($M_w > 4$) aftershocks tend to cluster in the region of moderate values of coseismic slip between the coseismic and postseismic slip zones, tending towards the latter (e.g., (Hsu et al., 2006; Agurto et al., 2012; Ozawa et al., 2012; Lin et al., 2013)).

The central part of the megathrust associated with its locked region (the LRZ in Fig. 4) or with a coseismic slip region (Fig. 5), where the largest interplate ruptures appear, spreads from a depth of ~15 to 45−55 km in a band that is several hundred kilometers wide. There is a tendency in inversions of static terrestrial displacements of the GPS-points due to strong earthquakes to locate the greater slip values primarily near the central part of the megathrust, while the seismic and tsunamigenic inversions show 50−80-m displacements near the uppermost part of the megathrust (Chlieh et al., 2007; Lay et al., 2012). For example, the smallest part of the rupture during the 2011 Tohoku earthquake behaved like a tsunamigenic earthquake. On the contrary, during the 2010 Maule earthquake in Chile, the rupture did not reach the oceanic trench (Lay et al., 2010; Vigny et al., 2011).

The results of observations of the seismic and deformation effects during the strong megathrust earthquakes show that the friction properties of the megathrust are heterogenous. This allows seismic and aseismic slips to interlay and interact from the oceanic trench axis to the very end of the activated surface of the megathrust at a depth of ~100 km. Heterogeneity is most likely determined by large variations in pressure; temperature; amount of pore fluids; properties of sedimentary deposits; and asperity and geometry of the fault, as well as its maturity, mineralization, and the type of rocks along a seismogenic part of the zone in the subducting megathrust fault (Lay et al., 2012).

The behavior of the upper 5−10 km of the megathrusts, overlapped usually by the corresponding accretionary prisms, is perhaps best known. This region of the megathrusts is usually considered aseismically adjusted to relative motions of the plates. This was caused by the presence of the bottom near-trench sediments that undergo large inelastic strains. Eventually, these strains increase the friction properties of the megathrust, impeding the origination of seismic instability and thereby providing a total low level of seismicity within the accretionary prism. Nevertheless, this small region is subject to discontinuous large-scale ruptures, which lead to the appearance of the tsunamigenic seismic destruction of a megathrust up to the surface. The tsunamigenic Tohoku earthquake is a bright example.

Further, in its lowest part, the megathrust displaces aseismically along the fault, which suggests the change in friction properties of the fault that provides the transition from the brittle to brittle-plastic failure. This is partly confirmed by the observations of episodic events of slow aseismic slip ("quiet" or "slow" earthquakes) and "seismic tremor" in the form of continuous sequences of seisms of low intensity in some regions of the world (particularly in southwestern Japan and southern Chile) (e.g., (Beroza and Ide, 2011; Ide, 2012; Idehara et al., 2014)).

In recent years, due to the occurrence of these catastrophic subduction earthquakes, data has appeared on the existence of systematic differences of seismic radiation of aftershocks with respect to their depth in the center of the megathrust, which suggests the possibility of its separation into upper and lower halves with respect to this feature (Lay et al., 2012; Koper et al., 2012).

The essence of this approach is considering the inverse projections of short-period signals in the megathrust plane at the dense seismic networks with broadband recording in the teleseismic zone using the procedure developed in (Xu et al., 2009). According to this procedure, the seismic records at the selected group of stations with a relatively uniform spatial distribution and high quality of data are aligned by multistation cross-correlation and are filtered by narrowband filtering with a central period of 1 s. Then, based on the reference Earth model, the travel time is calculated for each station from each node in the network of forming the images of the source region on the
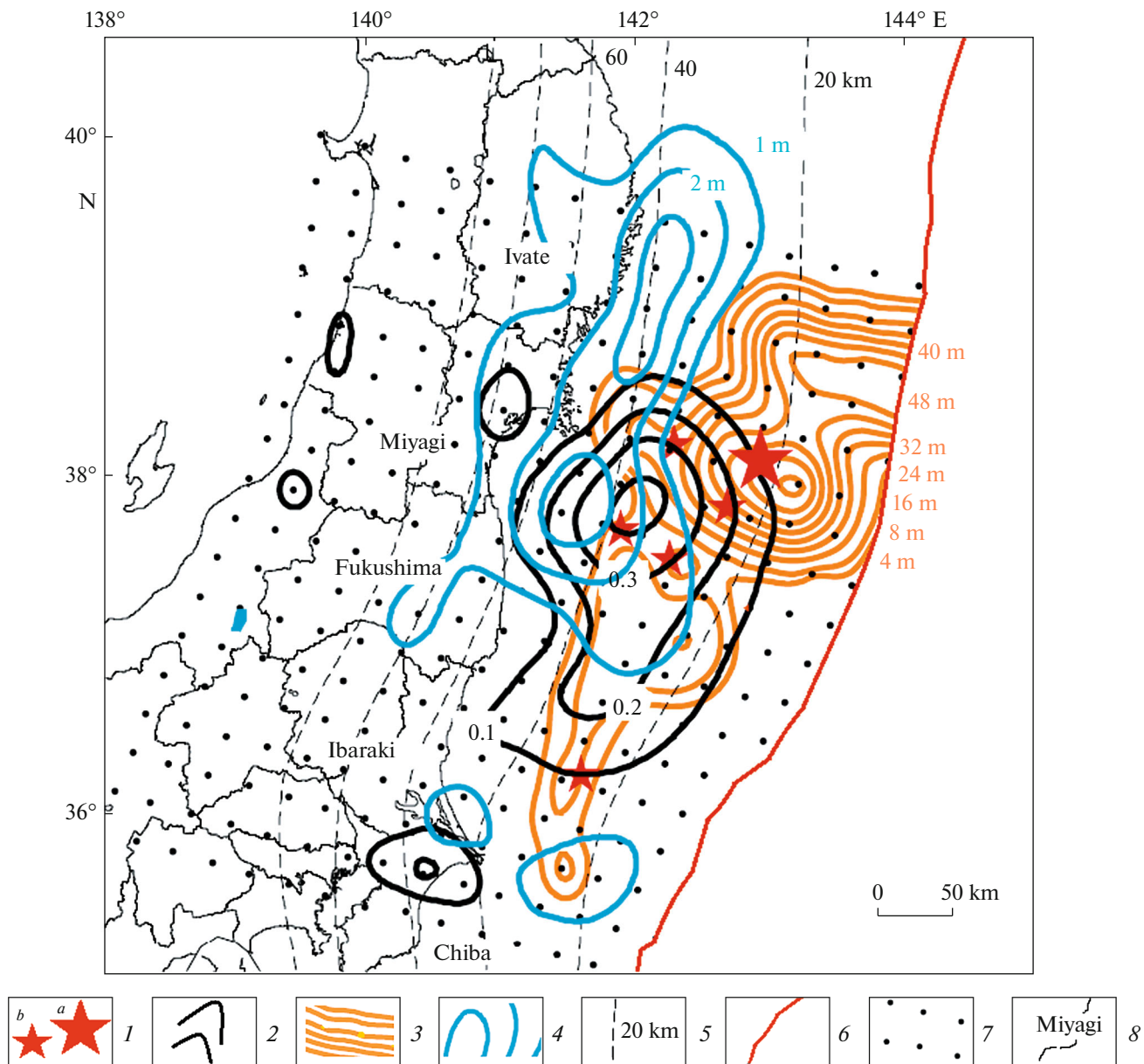
Fig. 6. Distribution of regions of preseismic, coseismic, and postseismic slip in spacetime neighborhood of the 2011 Tohoku earthquake ($M_w = 9.0$) determined by the data of GPS measurements (modified Fig. from (Ozawa et al., 2012. Fig. 12)). (*1*) (*a*) Epicenter of the Tohoku earthquake and (*b*) epicenters of the strongest events ($M_w = 6.5-7.1$) over the preceding period of 2003−2011, (*2*) region of preseismic slip for 2003−2011, (*3*) region of coseismic slip (1 day after the earthquake), (*4*) region of postseismic slip (March 12, 2011−October 12, 2011), (*5*) depth contours of the subducting plate surface, (*6*) axis of Pacific Ocean trench, (*7*) centers of the 20 × 20 km sites for the determination of the indicated slip regions, and (*8*) prefectures in Japan.

megathrust plane. Next, the traces of the data signals are aligned by the earlier part of the signal and offset from each point of the network according to a relative displacement predicted in the calculations. Then, the powers of ray beams are summated. Thus, a 2D spatial network of time variations in the power of ray beams of short-period radiation is constructed. This image is compared to a region of maximum coseismic slips reconstructed by a set of seismic, geodetic, and tsunamigenic data.

Figure 7 compares the relative position of the regions of coherent high-frequency radiation concentration and the regions of maximum coseismic slip for three great subduction earthquakes considered.

In each of three cases, coherent short-period radiation is generated from the lower part of the megathrust closest to the coast (a depth of 25−50 km), while the zones of the maximum coseismic slip are found in the upper 25 km, extending towards the sea closer to
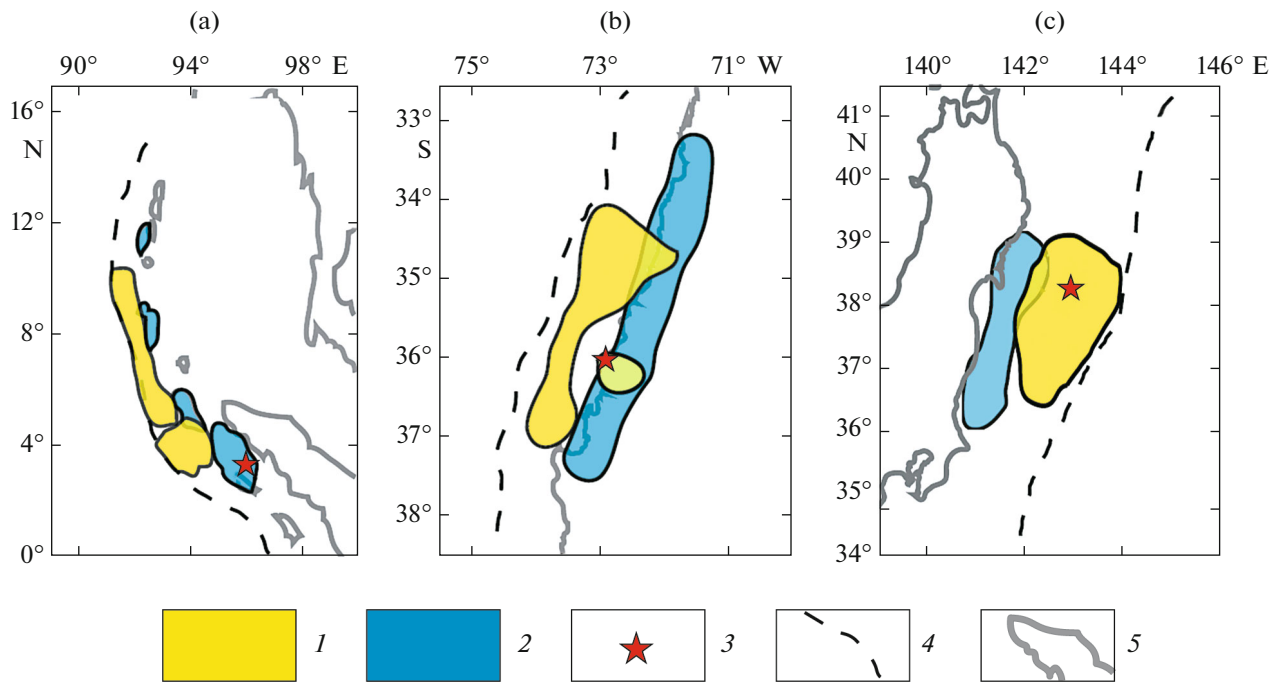
Fig. 7. Schematic generalization of the images of maximum coseismic slip and coherent short-period (~1 s) radiation in the teleseismic zone for three great subduction earthquakes: (a) Sumatra of December 26, 2004, Indonesia ($M_w = 9.2$); (b) Maule of February 27, 2010, Chile ($M_w = 8.8$); and (c) Tohoku of March 11, 2011, Japan ($M_w = 9.0$) (modified Fig. from (Lay et al., 2012, Fig. 5)). (*1*) Coseimic slip, (*2*) coherent short-period (~1 s) radiation, (*3*) epicenters of strong earthquakes, (*4*) position of the oceanic trench axis in the subduction zone, and (*5*) coastline.

the trench. At the same time, in the first two cases (the Sumatra earthquake and the Maule earthquake), the hypocenter of the main shock was located in the lower zone of coherent short-term radiation and the hypocenter of the main shock of the Tohoku earthquake was located in the upper zone of maximum coseismic slip. During the Tohoku earthquake, the greater part of the boundary between the Pacific and Okhotsk plates ruptured near the Tohoku coast. The initial duration of the process (about 150 s) included the rupture of the region of a very large coseismic slip (from 30 to 60 m) on a small segment of the megathrust (Tajima et al., 2013; Wang et al., 2018). It is likely not fortuitous that, during this earthquake, the maximum height of the tsunami wave reached 30−40 m at about 200 km along the Sanriku Coast and extended 10 km deeper into the dryland (Lay and Kanamori, 2011). At the same time, during the stronger Sumatra earthquake, the maximum height of the tsunami wave did not exceed 10 m and then only at a limited segment of the coast in the Aceh area (Lay et al., 2005).

The confinedness of coherent high-frequency radiation to the greater depths on the surface of the megathrust can be interpreted as the demonstration of a change in friction properties on its surface with depth. The upper part of the megathrust turns out to be relatively smoother, which manifests itself in the confinedness to relatively shallow depths of the maximum values of the coseismic slip, while at the deeper

surface of the megathrust there is a large number of small asperities which contribute to high-frequency seismic radiation.

CONCEPTUAL MODEL OF MEGATHRUST RUPTURE

It was shown above that the character of displacements on the megathrust surface depends considerably on the subduction depth. A conceptual model, consisting of four types of displacements on the megathrust surface, was developed in (Lay et al., 2012). These types (domains) with different seismic behaviors are shown schematically in Fig. 8. The shallowest region of the megathrust (domain A) extends from the trench to a depth of 15 km below sea level and undergoes either a seismic strain or large coseismic displacements during tsunami earthquakes. If a large coseismic slip occurs at a shallow depth during a megathrust tsunamigenic earthquake, it is not clear if the destruction strain is distributed to the surface of the fault end or focused at the low end of domain A and further upward the displacement occurs aseismically.

Strong earthquakes in domain B (at a depth from 15 to 35 km) are caused by the brittle failure of the megathrust surface with a large total value of coseismic slip, at which relatively modest amounts of coherent short-period energy are radiated. Strong earthquakes that destroy domain C (the depth from 35 to 55 km) are
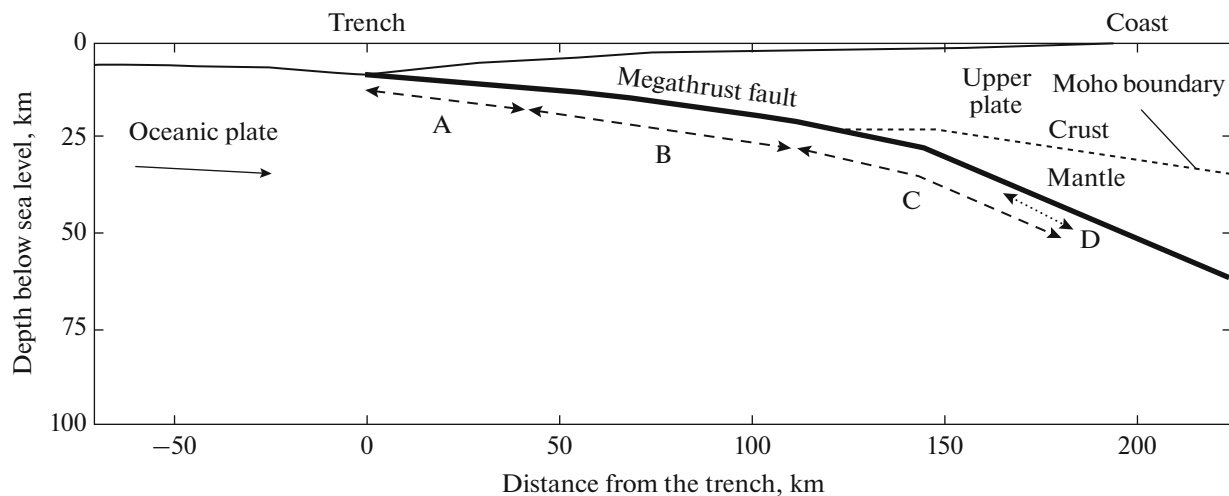
Fig. 8. Conceptual model of the megathrust rupture (modified figure from (Lay et al., 2012. Fig. 6)). (A) Domain nearest to the trench (type), in which tsunamigenic earthquakes or inelastic deformations and stable aseismic slip occur; (B) central megathrust type, in which maximum coseismic slip occurs during insignificant short-period seismic radiation; (C) subducting type, in which a moderate slip occurs during significant coherent short-period seismic radiation; (D) transition type from brittle to brittle−plastic failure, in which the events of slow aseismic slip, low-frequency ("quiet" or "slow") earthquakes, and "seismic tremor" develop simultaneously. At even greater depths, a megathrust slips aseismically stably, either with episodic slow slip or with plastic deformation that does not generate any signs of seismicity.

accompanied by a moderate coseismic slip but a relatively large amount of radiated coherent short-period energy. This is a rather subtle difference, and the evidences of such segmentation in the rupture properties result primarily from the detailed analysis of the catastrophic earthquakes in Sumatra in 2004 ($M_w = 9.2$), in Chile in 2010 ($M_w = 8.8$), and in Tohoku in 2011 ($M_w = 9.0$) carried out in (Lay et al., 2012).

The final megathrust domain (D) is a transition region from brittle to brittle−plastic/plastic failure in the lowermost part of the megathrust, where a slow slip, low-frequency events, and seismic tremor phenomena occur. As we mentioned, such phenomena are observed at these depths in reality (e.g., (Beroza and Ide, 2011; Ide, 2012; Idehara et al., 2014)).

CORRELATION BETWEEN THE ORIENTATION OF THE SLIP PLANE IN THE SOURCES OF GREAT SUBDUCTION EARTHQUAKES AND THE PLANE OF A CORRESPONDING MEGATHRURST

At present, there are no reliable criteria for unambiguously selecting the slip plane from two possible planes according to the focal mechanism (FM) solution or centroid moment tensor (CMT). Nevertheless, in the case of great subduction earthquakes, it is possible to select one of two solutions of the slip plane ("working plane") using the information on the spatial structure of their aftershocks together with the known configuration of the plate boundary in the subduction zone.

Figure 9 presents the CMT solutions (according to the Harvard CMT Catalog (Dziewonski et al., 1981;

Ekström et al., 2012)) for the catastrophic earthquakes under discussion. We recall that the Lode−Nadai coefficient of these earthquakes is not equal to zero, but is represented by small negative values of the solutions for the Sumatra and Maule earthquakes (−0.045 and −0.059, respectively) and a small positive value of the solution for the Tohoku earthquake (+0.004) (Fig. 9).

The numerical values of the CMT solutions for the earthquakes under discussion are listed in Tables 1 and 2 (the lines in the GCMT catalog). The epicentral data of these earthquakes and numerical values of the parameters of their focal mechanisms are duplicated in the tables according to the data from the NEIC and ISC catalogs.

The differences in the epicenter coordinates are the greatest between the values in the GCMT catalog compared to the ones in the NEIC and ISC catalogs, reaching 0.8° in latitude and 1.5° in longitude. The differences in the depth values calculated are less significant. The epicentral differences are explained by the fact that, during the construction of the CMT solution, the hypocenter coordinates may differ significantly to reach the best coincidence of the real and comparable estimated waveforms of seisms. Nevertheless, the focal mechanism solutions themselves presented in Tables 1 and 2 turn out to be quite similar for a certain earthquake according to the data from the different catalogs.

It follows from Fig. 9 and Tables 1 and 2 that the CMT solutions for all three earthquakes under discussion are characterized by a near-horizontal (working) and a near-vertical nodal plane. In all cases, a flat surface subducts at small inclination angles (8°−18°).
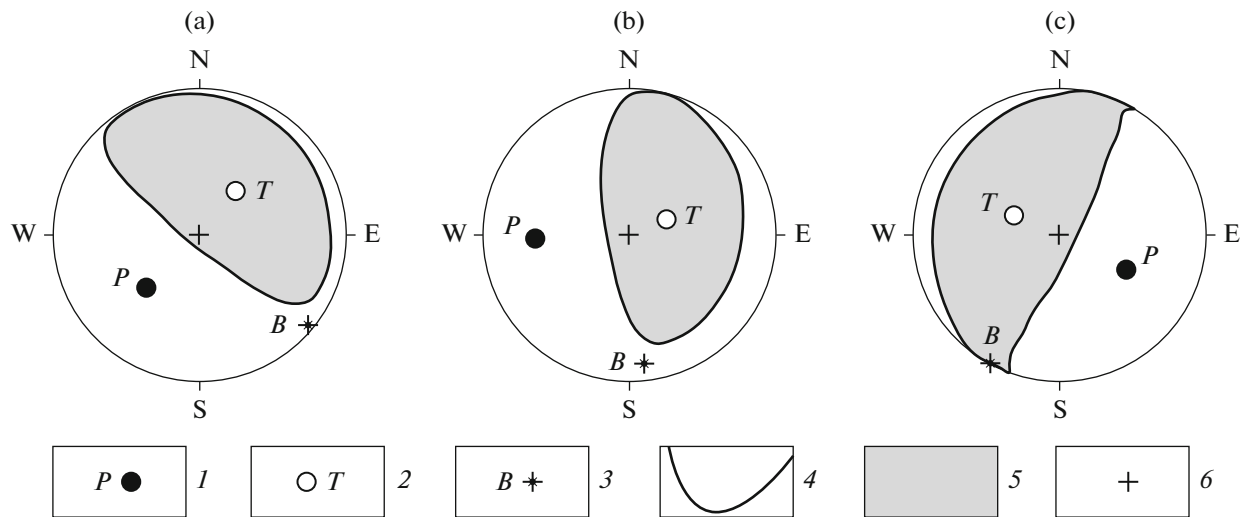
Fig. 9. CMT solutions for three great subduction earthquakes: (a) Sumatra of December 24, 2004 ($M_w = 9.2$); (b) Maule of February 27, 2010 ($M_w = 8.8$), and (c) Tohoku of March 11, 2011 ($M_w = 9.0$). (*1*) Emergence of principal axis *P* of compression (shortening) on the surface of the lower focal hemisphere, (*2*) emergence of principal axis *T* of tension (elongations), (*3*) emergence of intermediate axis *B* (hereinafter, we use the designation "*B*" instead of more widely used designation "*N*" due to historically formed practice of Russian constructions of focal mechanisms), (*4*) projection on the lower focal hemisphere of the nodal surface, (*5*) region of extension, and (*6*) center of equiangular stereographic projection.

These angles approximately correspond to the inclinations of the megathrust plane in three subduction zones. Since most of the aftershocks with thrust focal mechanisms are along these flat planes, it is reasonable to assume that these planes should be selected as working.

Due to the work (Araki et al., 2006), we can study in detail the kinematics of the motion in the source of the Sumatra earthquake using the data of high-accuracy observations by a dense network of 17 temporary seismic stations with an average distance of 15 km between them in February–March 2005 almost immediately after the main shock. The stations were located on a seismic profile 50–70 km wide across the

epicentral zone of this earthquake and across the strike of the trench passing at ~150 km northwestward from the earthquake epicenter. Figure 10 presents the epicentral sampling studied and shows a vertical section of the corresponding sampling of the hypocenters. It also displays a focal mechanism type for the Sumatra earthquake in a vertical projection according to (Scalera, 2007).

The concentration of aftershock hypocenters close in time to the main shock, which is well-pronounced at the indicated cross section in a relatively narrow band of the sampling under study, dips to a depth at a similar angle to dipping of the working plane in the source of the Sumatra earthquake. Therefore, the

Table 2. Orientation of the planes of CMT solutions for three great subduction megaearthquakes (December 26, 2004–March 11, 2011)

Region	Catalog	H, km	M_w	First (working) plane			Second plane		
				Strike, deg	Dip, deg	Slip, deg	Strike, deg	Dip, deg	Slip, deg
Sumatra	GCMT	29		329	08	110	129	83	87
	NEIC	30	9.2	274	13	055	130	79	98
	ISC	27							
Maule	GCMT	23		019	18	116	172	74	82
	NEIC	30	8.8	014	19	104	179	71	85
	ISC	23							
Tohoku	GCMT	20		203	10	88	025	80	90
	NEIC	24	9.0	193	14	81	022	76	92
	ISC	20		124	16	18	17	85	106

kinematics of the motion in the strong earthquake source is in a good agreement with the pattern of kinematics of the Indian oceanic lithosphere subduction beneath the Sunda arc (e.g., the lower section in Fig. 3).

FEATURES OF DAMAGE IN THE AFTERSHOCK SEQUENCE OF THE TOHOKU EARTHQUAKE

We pointed out earlier in (Lukk and Leonova, 2020) that, in the aftershock sequence of the Tohoku earthquake, the content of events with a fault type in their focal mechanisms, which is not typical of the setting of subhorizontal compression domination in the Japan zone of subduction, is unusually high. We mean not the seismic events from the ocean side of the trench, the presence of which here is considered evident due to the propagation of bending strains in the subducting oceanic lithosphere, but the events that occurred from the continental side of the trench near the coast of Japan. We note that this effect is absent in such an expressed form in the aftershock sequences of two other subduction earthquakes discussed here.

Figure 11 presents the distribution of the inclination angles with the horizon of the principal axes (compression P, tension T, and intermediate B) of the focal mechanisms in the aftershock series of three great earthquakes according to the data from the ISC catalog for events with $M \geq 5.0$ for the Sumatra and Maule earthquakes and with $M \geq 4.0$ for the Tohoku earthquake. The common point is the closeness of the distribution of the angles of inclination of axes B to the horizon for all three earthquakes. The corresponding axial traces (not shown here) indicate that, in all cases considered, the near-horizontal axes B lie in the plane of megathrusts trending in the same direction. An almost identical type of distribution of axes P (maximum near $15°-20°$ for the Sumatra earthquake and $25°-30°$ for Maule) and axes T (maximum near $70°-75°$ for the Sumatra earthquake and $60°-65°$ for Maule), together with their near-orthogonal orientation to the trench, point out that, in both cases, a type of focal mechanisms of the considered sets of aftershocks of these two earthquakes agrees with the domination of overthrust (underthrust) destruction in their aftershock zones. These results contradict the histograms of inclinations of axes P and T for the Tohoku earthquake shown in Fig. 11. Their two vivid humps indicate that, together with the overthrust (underthrust) focal mechanisms inherent to the aftershocks near the interface of the lithospheric plates, the fault focal mechanisms untypical of the megathrust surface are equally presented in the sampling considered.

In fact, such mechanisms were seldom observed in the aftershock series of the Sumatra and Maule earthquakes, but the regions of their distribution were strictly localized. For example, for the Sumatra earthquake, a noticeable region of distribution of aftershocks with fault focal mechanisms was the Anda-man—Nicobar zone of the pre-arc expansion in the northern tip of the fault zone (Dewey et al., 2007; Engdahl et al., 2007; Lukk and Leonova, 2018). For the case of the Maule earthquake, such aftershocks were clustered within the accretionary prism in the north, in the vicinity of Pichilemu (Farias et al., 2011; Lange et al., 2012; Melnick et al., 2012; Aron et al. 2013; Cubas et al., 2013), and partly beneath the Arauco Peninsula in the south (Lange et al., 2012; Melnick et al., 2012; Aron et al., 2013).

The large number of aftershocks with fault focal mechanisms after the Tohoku earthquake sharply differs from this relatively small number of similar events observed locally after two other strong earthquakes. The coexistence of earthquakes with a comparable number of fault and overthrust focal mechanisms within the same type of the stress-strain state is impossible in the same spatial sampling. Therefore, it is appropriate to examine them separately. To do this, we divided their full sampling in the aftershock period into two sets: with angles of inclination with the horizon of axes P equal to or less than $40°$ and with angles of their inclination greater than $40°$. The tensors of average focal mechanisms constructed by these two samplings, using the procedures by S.L. Yunga (1990), are shown in Fig. 12. The solutions obtained differ fundamentally. The solution in Fig. 12a (for angles equal to or less than $40°$) is rather consistent with the regime of dominance of overthrust—underthrust destruction in the Japan zone of subduction. The orientation of individual axes p and t, by which the orientation of principal axes P and T of the average mechanism is determined, is well-ordered.

At the same time, at a high degree of order of individual axes p (the solutions presented in Fig. 12b for the angles of inclination greater than $40°$), the individual axes t almost equally fill the entire possible range of azimuths. This indicates the high positive values of the Lode—Nadai coefficient (μ_m). Coefficient μ_m is used to characterize a type of seismotectonic deformation: its values change from -1 (uniaxial elongation) to $+1$ (uniaxial shortening) through 0 (pure shear). The result obtained here indicates a highly ordered vertical load (in the direction of compression axis P). The weight of the accretionary prism can be considered as such (Lukk and Leonova, 2020).

A few researchers believe that such a prism existed at shallow depths near the exposure of the rupture during the Tohoku earthquake (Zhao et al., 2011; Tajima et al., 2013; Yamamoto et al., 2014; Azuma et al., 2018). One distinctive feature of this segment in the accretionary prism is the higher values of the P and S wave propagation velocities compared to the neighboring segments at relatively shallow depths in the accretionary prism, which were calculated using seismic tomography at a set of dense seismic profiles (Zhao et al., 2011; Tajima et al., 2013; Yamamoto et al., 2014; Ito et al., 2017; Azuma et al., 2018). These
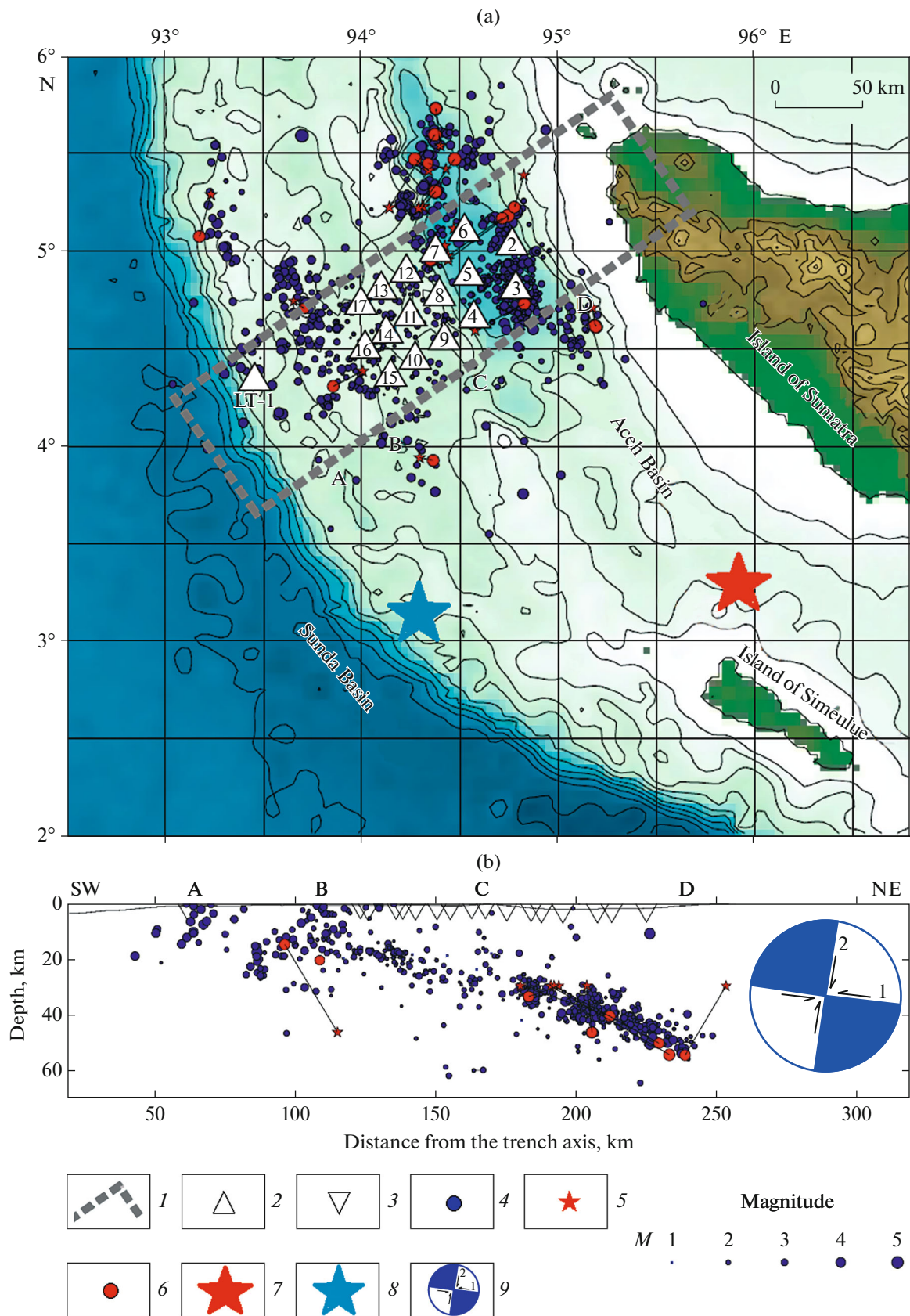
(a)

(b)

Fig. 10. (a) Epicentral sampling of the epicenters nearest in time to the main shock of the Sumatra earthquake aftershocks based on the data of high-precision observations in February–March 2005 and (b) their vertical section across the strike of the trench (modified figure from (Araki et al., 2006, Fig. 3)). (*1*) Epicentral sampling, (*2*) network of seismic stations of high-precision observations, (*3*) position of these stations on the axial line of vertical section, (*4*) position of high-precision hypocenters of aftershocks (the diameter corresponds to the magnitude), (*5*) position of isolated hypocenters from the USGS (ISC) catalog of primary processing of earthquakes by a global network of stations, (*6*) their redetermined position according to the data of dense high-precision network demonstrating the more compact extraction of the overthrust plane according to the high-precision observation data, (*7*) epicenter of the Sumatra earthquake according to ISC catalog, (*8*) epicenter of the seismic moment tensor for the Sumatra earthquake according to the Harvard catalog of CMT solutions, (*9*) projection on a vertical plane of the focal mechanism for the Sumatra earthquake according to (Scalera, 2007).
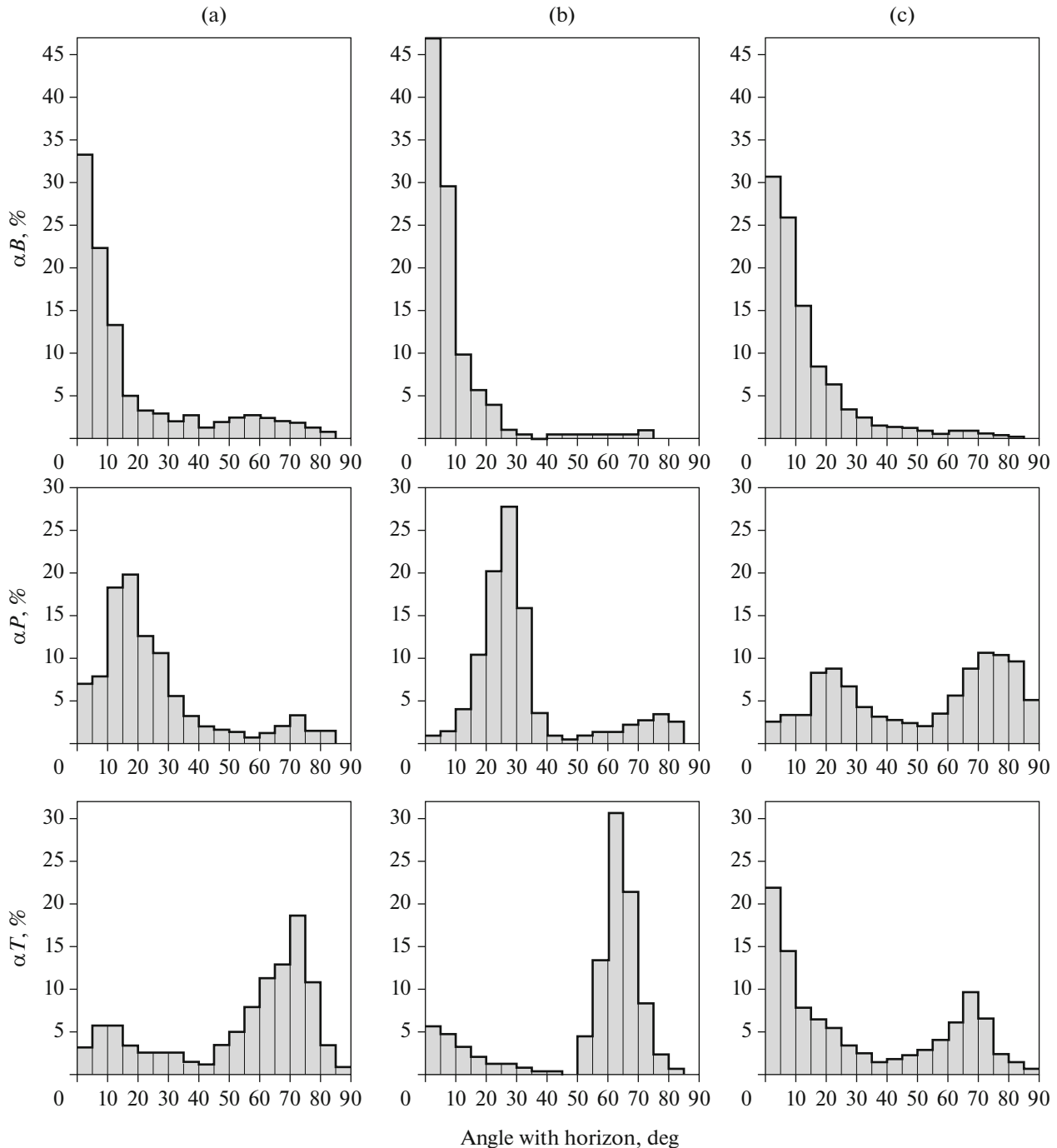

Fig. 11. Distribution of inclination angles with horizon of principal axes *T* (tension), *P* (compression), and *B* (intermediate) of focal mechanisms for the aftershock sequences of three great megaearthquakes: (a) Sumatra (December 26, 2004–December 31, 2005; *N* = 630), (b) Maule (February 27, 2010–December 31, 2012; *N* = 230), and (c) Tohoku (March 11, 2011–December 31, 2011; *N* = 664).
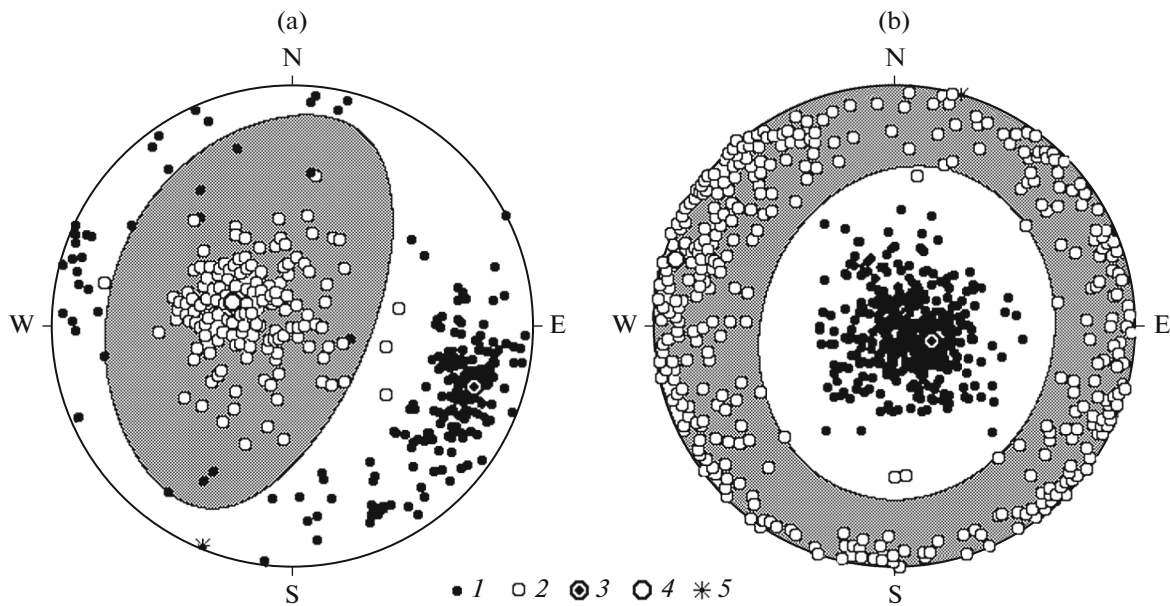
Fig. 12. View of the average focal mechanisms during the aftershock period (March 11, 2011–December 31, 2011) after the Tohoku earthquake, which were constructed by the procedure of S.L. Yunga (1990) based on two separate samplings with inclination angle of axes *p* (compression) of individual mechanisms (a) equal to or less than 40° and (b) greater than 40° (modified figure from (Lukk and Leonova, 2020, Fig. 8). (*1*) Emergence of principal axes *p* of compression of individual focal mechanisms on the lower focal hemisphere, (*2*) emergence of principal axes *t* of tension of individual focal mechanisms on the lower focal hemisphere, (*3*) position of principal axis *P* for the average mechanism solution, (*4*) position of principal axis *T*, and (*5*) position of intermediate axis *B*. The region of tension (elongation) is shaded on the projection of the focal hemisphere.

high velocity values are associated by the authors of the indicated research, with the back part of the accretionary prism (the paleoprism) located more closely to the trench at this segment and having a rigid core at shallow depths composed of strong rocks of Cretaceous age. Here, the frontal part of the accretionary prism composed of soft terrigenous deposits of Neogenic age (Tsuru et al., 2000, 2002) and crumpled into folds along a series of overthrust folds turns out to be strongly contracted compared to the similar segments of the accretionary prism, which are located northward and southward of the segment under discussion. Here, it is as if the middle part of the prism hangs over its frontal part, overlapping the latter along the low-angle overthrust, which is called a "backstop" in English the language literature. As a result, this part of the prism turned out to be much closer to the axial part of the trench than the neighboring parts of the accretionary prism adjoining it on the north and the south.

We note that, if the aftershocks with an overthrust type of the mechanism fill the broad vicinity of a destructive earthquake epicenter, including the region of maximum values of coseismic slip identified by the geodetic data (Geospatial Information..., 2011), then it is as if the aftershocks with a fault type of slip "avoid" this region, "pressing" against the coast of Honshu Island (Lukk and Leonova, 2020). In most cases, their hypocenters are located primarily at shallow depths (≤15 km) in the Earth's crust, while earthquakes with an overthrust type of slip are located in the lower part

of the Earth's crust and in the upper mantle with the maximum in the depth interval of 45−55 km near the surface of the subducting lithospheric plate (Lukk and Leonova, 2020).

DISCUSSION

A review of the data about the character of the motions in the sources of the catastrophic earthquakes in the subduction zones showed that they all, without exception, can be represented by backstops plunging beneath the continental part of the subduction. This also concerns two great subduction earthquakes: in Chile in 1960 (M_w = 9.5) and in Alaska in 1964 (M_w = 9.2) that occurred when instrumental observations were insufficiently representative. For example, it is explicitly stated in (Kanamori and Cipar, 1974) that the rupture in the source of the 1960 Chile earthquake is represented as a megathrust with a small angle (~10°) of dip beneath the continent. The megathrust, subducting at an angle of ~20° beneath the continent, determines the character of faulting during the earthquake in Alaska in 1964 in (Kanamori, 1970). A similar idea about the earthquake source in Alaska is given in (Plafker, 1969), where the earthquake source is described as a "complex megathrust descending at a small angle beneath a continental margin from the vicinity of the Aleutian Trench."
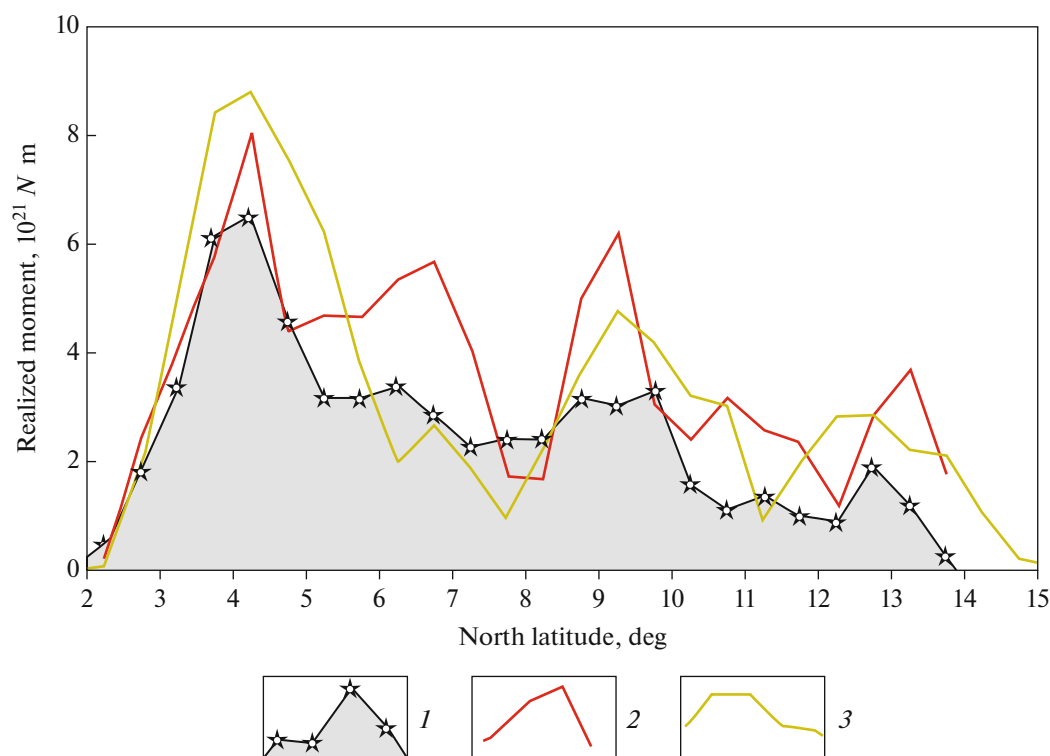
Fig. 13. Distribution of the scalar moment value with distance along the trend of the Sumatran fault plotted using the calculation models of rupture based on the seismological and geodetic data (modified figure from (Subarya et al., 2006, Fig. 4)). (*1*) Seismological model of rupture propagation, (*2*) geodetic model A of rupture propagation, and (*3*) geodetic model B of rupture propagation.

The comparative description of the characteristics of the great subduction earthquakes performed in this work suggests that, despite many common features in the release of elastic stresses accumulated for a long time due to the collision of lithospheric plates, there are also noticeable differences in some of their properties. Table 3 summarizes the important characteristics of the ruptures for all subduction earthquakes that occurred during the period of rather conditioned instrumental observations and have been known since 1964. The author's values of a seismic moment and released stresses in the case of other dimensions in the source of information are converted to dimensions N m and MPa.

In regards to seismic moment value, the great Chile earthquake of 1960 surpasses the other seismic catastrophes by half an order of magnitude. Nevertheless, the duration of rupture during this earthquake was much shorter than during the Sumatra earthquake of 2004. The duration of rupture during the Chile earthquake was also much shorter (almost by a factor of two) than the duration of rupture during the Sumatra earthquake.

The second greatest catastrophic earthquake in magnitude that occurred in Alaska in 1964 also exceeds the later seismic catastrophes in the seismic moment value by almost a factor of two. However, the

length and duration of the rupture (~340 s) are exceeded by the Sumatra earthquake, during which the rupture lasted for an exceptionally long time, 500–600 s. Thus, we recognize that the Sumatra earthquake of 2004 was an outstanding event according to these two parameters. This feature of the Sumatra rupture is explained by the fact that it might likely consist of several sources (Ishii et al., 2005; Subarya et al., 2006; Lay and Kanamori, 2011).

The corresponding time function of the source in the form of distribution of the scalar moment values with distance along the strike of the Sumatran fault, which is constructed by the calculated rupture models based on seismological and geodetic data, is presented in Fig. 13 according to (Subarya et al., 2006). It appeared that all distributions are similar in character for all estimated models and their common typical feature is the occurrence of three well-expressed extrema near 4°–5°, 9°–10°, and 13°–14° N.

Unilateral rupture during the Sumatra earthquake began in the hypocenter of the main shock westward of the northern tip of Sumatra Island near Simulie Island and propagated to the northwest at a rate of about 2.7–2.8 km/s for ~200–250 s. The first extremum of the time function of source radiation was observed near 80–100 s (according to Fig. 2 and the published work (Ishii et al., 2005)) and spatially at an

Table 3. Main parameters of destruction during the great subduction megaearthquakes

M_w	$M_0 \times 10^{22}$, N m	S_{drop}, MPa	L, km	W, km	T, s	Vr, km/s	Slip, m	Source
				Chilean, May 22, 1960				
9.5	27		800–1000		345	3.5		(Shearer and Bungmann, 2010)
	27		800	200	300–600	3.5	30	(Kanamori and Cipar, 1974)
				Alaskan, March 28, 1964				
9.2	7.5		700		340	3.0		(Shearer and Bungmann, 2010)
9.2	5.9		600	250			30	(Holdahl and Sauber, 1994)
	7.5	2.8	600			3.5		(Kanamori, 1970)
				Sumatran, December 26, 2004				
	6.5					~2.0	11.4	(Ammon et al., 2005)
9.2			1200		500	2.5		(Ni et al., 2005)
			1150		480–500	2.3–2.7		(Kruger and Ohrnberger, 2005)
			1100		480	2.3		(Lomax et al., 2005)
9.0			1235		515	2.0–2.7		(Guilbert et al., 2005)
9.3	13	>1	1300		600	2.8		(Ishii et al., 2005)
9.1	4.0		1300–1600		>500		5	(Lay et al., 2005)
9.2	7.0		1000		145	3.6	>20	(Vigny et al., 2005)
9.1	6.8	2–4	1300–1500	150	500		15–20	(Subarya et al., 2006)
9.2	7.0		1500		500–600	2.0–2.7	20	(Chlieh et al., 2007)
	4.0	0.3–2.5					>5	(Dewey et al., 2007)
9.0	3.5		1700	240	500	2.5–2.8		(Engdahl et al., 2007)
				Maule, February 27, 2010				
	2.1		550		120–140	2.0–2.5		(Lay et al., 2010
8.8	1.76		500	100		2.8–3.1	~15	(Vigny et al., 2011)
						2.0–2.6	~10	(Lorito et al., 2011)
8.8	2.0		450–550		120–140	2.5–3.5		(Koper et al., 2012)
8.8		4.9	600–650	200				(Aron et al., 2013)
						1.5–2.75	15–20	(Hayes et al., 2013)
8.8	2.2		460	100	100–120	2.5–3.0	~15	(Lin et al., 2013)
				Tohoku, March 11, 2011				
8.9	2.8		250	120	140	2.1	54	(Hao et al., 2011)
	2.9	15–30		160	150	1.0–2.5	60–80	(Lay and Kanamori, 2011)
9.0	3.9		320	180		1.5–2.5	63	(Lay et al., 2011)
9.0	3.4		400	100			>27	(Ozawa et al., 2011)
9.1	5.7		500	200	180	1.5	60	(Shao et al., 2011)
9.0	3.9	10			60–120	1.5	40–60	(Lay et al., 2012
					160–180	1.7–3.5		(Kiser, Ishii, 2012)
9.1	3.8–4.6		240				>10	(Wang et al., 2012)
8.9	2.2–3.8		500	180	150	1.8–2.0		(Zhang et al., 2012)
9.0	4.5 × 10				150		30–60	(Tajima et al., 2013)
9.0		6–14					40–60	(Wang et al., 2018)

M_w, moment magnitude; M_0, total scalar seismic moment; S_{drop}, released stresses; L, rupture length; W, calculated width of the rupture plane; T, rupture duration; Vr, estimated velocity of rupture propagation; Slip, maximum value of coseismic slip.

interval of $4°−5°$ N (Fig. 13). The spatial position of this extremum corresponds to the Aceh basin located westward of the northern tip of Sumatra Island (Fig. 1a, Fig. 10). Here, we note that, during the Sumatra earthquake, the highest tsunamigenic wave occurred in the Aceh area and almost disappeared near the Nicobar Islands (Lay et al., 2005). Then, in the time function of the source at the point of about 300 s (Fig. 2), the second sudden extremum occurred, corresponding spatially to the Nicobar Islands ($9°−10°$ N, Fig. 13), where the rupture velocity noticeably decreased (from $2.7−2.8$ to 2.0 km/s) according to (Chlieh et al., 2007). We note that a strong tsunamigenic earthquake with $M_w = 7.9$ occurred here in 1881 (Ishii et al., 2005), the information on which can be used as an assumption about the existence of strength asperity on the Sumatran fault at that place. Finally, the third, less noticeable, extremum on the distribution of a scalar moment with distance falls onto the region of a well-expressed extension of the Andaman Basin.

The differences in the character of seismic radiation allowed some researchers to suggest that the first extremum of the distribution that was analyzed could have been determined by the existence of a secondary source related to the rupture of the megathrust segment in the Aceh Basin that created a large tsunami in it (Banerjee et al., 2007; Sibuet et al., 2007; Shearer and Bungmann, 2010).

It seems possible to develop this assumption by representing the Aceh area as a rigid formation that prevents the rupture propagation along the Sumatra overthrust during the Sumatra earthquake. It is as if the rupture stops for a moment at this rigid obstacle but then destroyed it with energy that was not depleted completely, which thereby caused a separate independent displacement of the overthrust in the form of an independent subearthquake that manifested itself in the significant expansion of the time function of the source. This assumption is also confirmed by a large value of released stresses at this obstacle. If the release of stresses in most of the Sumatran fault did not exceed the value of 0.5 MPa, then in Aceh it was 2.5 MPa (Dewey et al., 2007). It is also appropriate to note that a compact region of aftershocks with a shear-cutting slip (both principal axes P and T are tilted at angles close to $45°$) that are nearest in time to the main shock was located in the earthquake source, which is represented well by a group of focal mechanisms with a steep orientation of tension axis T in Fig. 1a; the same orientation was also observed for compression axis P (Engdahl et al., 2007). Under such mechanisms, one slip plane is subhorizontal and another is subvertical. Such high orderliness of aftershocks by the type of slip suggests an idea about the deformation of the study region in the epicentral zone of the Sumatra earthquake as a single whole.

The next extremum of distribution of the scalar value moment between $8°$ and $10°$ N can be deter-

mined by a similar process of the appearance of an additional subsource at the border between the Nicobar and Andaman Islands. As we noted, one of the strongest earthquakes in the Sunda arc with $M_w = 7.9$ occurred here in 1881 (Ishii et al., 2005). It is likely that this earthquake and the corresponding spike at the distribution of the scalar moment (Fig. 13) are related to the presence of a rigid barrier in this region similar to that in the Aceh region. Such arguments can also be given for the third extremum, in whose spatial neighborhood an earthquake with $M_w = 7.7$ occurred.

Based on the directional change in the dominant type of slip along the Sumatra rupture from south to north, it was suggested in the works (Rebetskii and Marinin, 2006a, 2006b) that a rupture should be represented as a complex process consisting of two stages. The rupture started at a depth of ~30 km and propagated upward along the backstop about 350 km wide from the northern tip of the Sumatra Island to the Nicobar Islands as a typical subduction megathrust earthquake. Then, it pulled apart a crustal-mantle body of the subduction zone in the form of a right lateral strike-slip along the Sumatra−Andaman fault and propagated up to the extension zone in the Andaman Basin. This idea does not contradict the analysis of the spatial distribution of the types of focal mechanisms performed in (Engdahl et al., 2007) for the Sumatra earthquake aftershocks in the same orientation from south no north (this can be partly seen in Fig. 1a).

Thus, the Sumatra earthquake is a unique event that falls out of a regular series of subduction earthquakes, despite the fact that it turns out to be comparable with one of the strongest known earthquakes, the catastrophic event of 1964 in Alaska, with respect to a total seismic moment and magnitude.

The second intense earthquake in recent times is the 2011 earthquake in Tohoku, which is similar to the Sumatra earthquake in magnitude and total seismic moment, has shorter rupture length by approximately three orders of magnitude, and is characterized by a noticeably smaller velocity of rupture propagation. However, the most noticeable difference of the Tohoku earthquake from the other seismic events discussed here is the unusually high values of maximum coseismic slip. They were observed in the form of a set of contours from 15 to 60 m within a rather compact zone. The length of this zone along the rupture did not exceed 200 km, and it lay downward on the gently dipping rupture plane almost from the seafloor near the trench, reaching $30−80$ km from it, at a depth of ~30 km. The earthquake hypocenter was in its lower part (e.g., Fig. 6, and published works (Hao et al., 2011; Lay et al., 2011; Lee et al., 2011; Ozawa et al., 2012; Zhang et al., 2012; Tajima et al., 2013)).

The identification of the compact zone of such large values of coseismic slip in the neighborhood of the epicentral region of the catastrophic Tohoku earthquake was far from being a trivial fact. The seis-

mological and geological studies performed in the territory of Japan before this earthquake in the vicinity of its future source suggested that, in the case of a catastrophic event in the subduction zone at this segment, the accompanying values of a coseismic slip cannot be significant. The low values of rigidity for unconsolidated sedimentary rocks and small friction coefficients in the frontal part of the accretionary prism at the internal slope of the trench were stated as the primary cause (Bilek and Lay, 1999; Tsuru et al., 2000, 2002). If a catastrophic earthquake were to be assumed to occur in the near future, its epicenter would be located markedly south of the Tohoku region (Tsuru et al., 2002). Such a possibility of a future seismic catastrophe by approximately 3°–4° lower than the epicenter of the Tohoku earthquake is indicated in one of the latest studies of the properties of low-frequency seismic noise in the islands of Japan from early 1997 through March 2018 using a new procedure of estimating dynamic seismic hazard (Lyubushin, 2018).

Nevertheless, we deal with the 2011 Tohoku earthquake. The maximum values of coseismic slip observed during this earthquake were recorded for the frontal part of the accretionary prism located here much closer to the trench axis when compared to the northward and southward segments.

The frontal part of the accretionary prism, composed of Neogenic soft terrigenous deposits (Tsuru et al., 2000, 2002) and crumpled into folds along the series of overthrust faults, was strongly shortened compared to the similar segments of the accretionary prism located northward and southward of the segment considered and was in a high stress state before the earthquake. The almost complete absence of aftershocks at shallow (<20 km) depths recorded in (Lukk and Leonova, 2020) in the zone of maximum values of coseismic slip was explained in terms of total relaxation of stresses accumulated during the preparation of the Tohoku earthquake within the accretionary prism discussed (in its relatively rigid and strong middle part). We note that, according to the results of special seismic tomography works, it was determined that the propagation velocities of elastic waves are ~6% higher in the rocks composing this prism than the normal values and lower by ~6% in the rocks northward and southward of the prism (Zhao et al., 2011; Tajima et al., 2013).

It is suggested that the appearance of untypical aftershocks with a fault type of a focal mechanism at shallow depths in a broad vicinity of the discussed zone of elastic stress relaxation within the accretionary prism (Figs. 10, 11) should be explained with regard to appearance of intense subhorizontal tensile stresses in the upper part of the Earth's crust around this zone (Lukk and Leonova, 2020). In our opinion, these stresses cause fault slips that are untypical of the subduction zone in the aftershock sources with depths shallower than 20 km, which amount to at least 50% of

the total number of Tohoku earthquake aftershocks. The aftershocks of this type during the earthquakes in Maule and in Sumatra are a negligibly small fraction of their total number, which makes a fundamental difference of the aftershock process observed during the Tohoku earthquake.

The essence of such significant differences remains unclear. There are opinions that a major role is played by the geological structure of the accretionary prism and the thickness of sediments entrapped to the interplate space (Contreras-Reyes et al., 2010; Lay et al., 2012; Cubas et al., 2013; Tajima et al., 2013; Azuma et al., 2018; Wang et al., 2018). For example, the significant differences in intensity of postseismic slip in the epicentral zones of the catastrophic Tohoku and Sumatra earthquakes in 2011 and 2014, respectively, were proposed to relate to the compact form of the accretionary prism with a width of the frontal part of less than 300 km during the Tohoku earthquake in contrast to the extended frontal part of the prism in the case of the Sumatra earthquake (Wang et al., 2018). The processes of accretion and subduction of sediments and the consequences of these processes for megathrust seismicity were considered in detail for the catastrophic megathrusts in Chile in (Contreras-Reyes et al., 2010).

It should be recognized in any case that the geological structure of the accretionary prism in the suture zone between the lithospheric plates can play a noticeable role both in the process of elastic stress accumulation at the stage of preparation of a catastrophic earthquake and at the stage of relaxation, like in the case when numerous events with a fault type of a focal mechanism occurred in the aftershock sequence of earthquakes at shallow depths during the Tohoku earthquake.

The issue of the megathrust exposure in the region of the accretionary prism displaced towards the trench can be associated with the increased tsunamigenicity of this segment in the megathrust. It is not fortuitous that the tsunami wave observed during the earthquake in Tohoku reached the maximum amplitude of 40 m (Lay et al., 2011). Figure 14 presents the distribution of the height of the tsunami surge wave and the inundation level it caused on the coast. The maximum heights of the tsunami wave are recorded for the frontal segment of the accretionary prism; its approximate position is shown in Fig. 14 according to (Zhao et al., 2011; Tajima et al., 2013). Here, it is relevant to note that, in the bottom half of the accretionary prism shown in Fig. 14, the rigid "seismic asperity" region of Miyagi-oki was extracted according to the data of instrumental observations of the strong motions during the relatively strong earthquakes ($M \geq 7$) that have occurred in Japan since 1930 (Yamanaka and Kikuchi, 2004; Ozawa et al., 2012). This coincidence is hardly fortuitous.
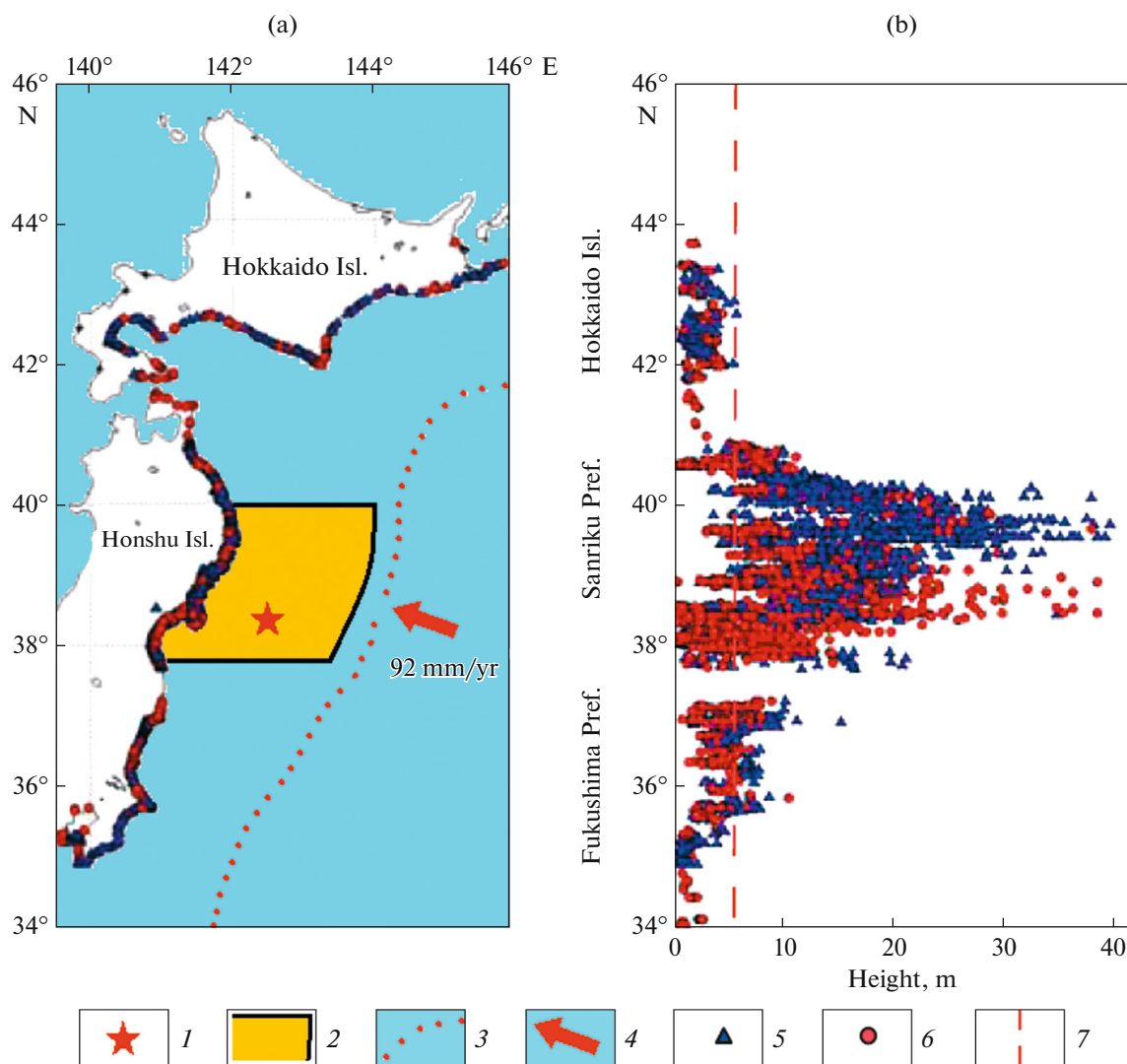
Fig. 14. (a) Relative location and (b) height of tsunami inundation during the 2011 Tohoku earthquake (modified figure from (Lay and Kanamori, 2011, Fig. 1)). (*1*) Epicenter of the main shock during the Tohoku earthquake (according to the ISC data): (*2*) approximate position of the accretionary prism discussed in the work according to (Zhao et al., 2011; Tajima et al., 2013), (*3*) approximate position of the oceanic trench axis, (*4*) orientation of motion of the subducting Pacific Plate, (*5*) maximum height of the tsunami surge wave, (*6*) maximum inundation level on the coast, and (*7*) height of the antitsunami wall of the Fukushima Nuclear Power Plant.

We discussed above the situation with the position of the smallest megathrust region (domain A), trending from the trench to a depth of 15 km, in the upper portion of which lies an accretionary prism (Fig. 5). A question arose as to whether the failure strain spreads to the surface end of the fault or focuses on the lowest end of domain A, and then upward the displacement is aseismic. In view of the above consideration, the first assumption would rather be taken for the case of the Tohoku earthquake, since here the accretionary prism was destroyed almost to the surface. This is likely to determine the unusually high tsunamigenicity of this seismic catastrophe.

The differences in the region of the development of the earthquake source for three catastrophic seismic

events were also observed during the study of the features of the stress field in their vicinity by cataclastic analysis, which is characterized by the possibility of determining not only the orientation of the principal stress axes, but also the calculation of relative stress values (Rebetskii, 2003). If a pressure gradient is located along the strike of a seismofocal region for the earthquakes in Sumatra and Maule (Rebetskii and Marinin, 2006a, 2006b), then, for the Tohoku earthquake, the vector of the stress gradient is oriented in its source area across the seismofocal region, in which case the stress level decreased primarily along the dip of the seismofocal zone (Rebetskii and Polets, 2014).

Finally, it should be acknowledged that the strength barriers and asperities on the surface of the

megathrust manifested themselves in particular geological structures, such as the accretionary prism in Tohoku or the faults oblique to the main rupture in Chile, or some rigid partitions at the different segments of the Sumatran fault may play a noticeable role in the formation of seismic effects during subduction megathrust earthquakes, making them remarkably unique.

CONCLUSIONS

This review of the published works concerning the seismic and deformation effects observed during all subduction megaearthquakes with magnitudes of ~9 and greater over the instrumental observation period suggests the following conclusions.

In all cases considered in this work, the main rupture was located during the earthquake in the corresponding subduction zone on the oceanic lithosphere surface subducting gently beneath the continent or the island arc. For an extended period, this zone is marked by the hypocenters of numerous weak earthquakes forming a seismogenic zone with a variable inclination in depth, called a Benioff zone in the seismological literature. During megathrust earthquakes, the slip plane is located on the upper flat segment of the Benioff zone. This segment is likely to be locked for a few hundred years before a megaearthquake with magnitude about 9 occurs, which is shown by a significant decrease in seismic activity in its area (the absence of seismic events with magnitudes smaller by about an order of magnitude than the main shock magnitude: "seismic quiescence").

This locked segment of the future rupture extends from several kilometers beneath the ocean floor to 30−40 km deep in the upper mantle during a strong earthquake. The trace of the rupture spreads on the surface during the catastrophic subduction earthquakes from 400−600 km in the case of the Tohoku and Maule earthquakes to ~1500 km during the Sumatra earthquake. This might have been caused by the specific geometry of the subduction zone, including the presence of an isolated microplate and strength barriers on the opposite ends of the rupture.

One of the two planes of the focal mechanism (sometimes called a working plane) is inclined at small angles (10°−20°) beneath the continental subduction part with a vector of slip normal to the oceanic trench, which is in full agreement with the subduction of the flat segment of the Benioff zone. This makes it possible to characterize the process of destruction in the catastrophic earthquake source as a megathrust, which destroys the previously locked segment of the Benioff zone. Most of the elastic energy that accumulated during the previous long-term deformation of the lithospheric plate collision zone is released here, which, in turn, is accompanied by the large values of coseismic slip determined by the geodetic observations.

During the Maule and Tohoku earthquakes, the rupture was bilateral, with its nearly symmetrical propagation from the epicenter; during the Sumatra earthquake, the rupture propagated from the epicenter unilaterally from southeast to northwest. The rupture duration was also different. If it was 140−160 s in the first two cases, it lasted unusually long for the Sumatra earthquake, up to 500−600 s.

Sometimes the rupture of the megathrust surface is exposed on the sea floor near the trench, causing the formation of a destructive tsunami wave. A vivid example is the Tohoku earthquake, which led to the destruction of the coastal accretionary prism. However, in some cases, a slip along the uppermost part of the overthrust occurs aseismically, not causing the rupture of the sea floor and the formation of a tsunami wave. This likely occurred during the Maule earthquake.

The rupture during the subduction earthquakes is not limited in depth by the previously locked seismogenic segment, marked by the region of the aftershocks nearest in time and the zone of maximum coseismic slips identified by the GPS measurements. Below the region of the coseismic slip lies the zone of concentration of coherent short-period (~1 s) radiation, which can be interpreted as an "aspirate" megathrust surface with a high degree of cohesion. Then, according to the geodetic measurements, the rupture continues aseismically (postseismic slip) in the transition zone from a brittle to brittle−plastic slip down to a depth of ~60−80 km (e.g., (Lin et al., 2013)). In addition, there are data that slips on the megathrust may also go slightly deeper to the region of brittle-plastic slip (e.g., Fig. 8 taken from (Lay et al., 2012)), which may be confirmed by the episodic events of slow slip ("silent" or "slow" earthquakes) and the "seismic tremor" observed in southwestern Japan and Southern Chile (e.g., Beroza and Ide, 2011; Ide, 2012; Idehara et al., 2014). These differences in seismic and deformation effects may evidence the significant changes in friction properties with depth along the megathrust surface.

It should be also acknowledged that the strength barriers and asperities on the surface of the megathrust, which manifested themselves in particular geological structures or in high-frequency radiation segments with an origin that is not clear yet, may considerably vary seismic effects during great subduction earthquakes.

CONFLICT OF INTEREST

The authors declare no conflict of interest.

REFERENCES

Agurto, H., Rietbrock, A., Ryder, I., and Miller, M., Seismic-afterslip characterization of the 2010 $M_w = 8.8$ Maule, Chile, earthquake based on moment tensor inversion, *Geophys. Res. Lett.,* 2012, vol. 39, paper ID L20303.
https://doi.org/10.1029/2012GL053434

Ammon, C.J., Ji, C., Thio, H., Robinson, D., Ni, S., Hjorleifsdottir, V., Kanamori, H., Lay, T., Das, S., Helmberger, D., Ichinose, G., Polet, J., and Wald D., Rupture process of the 2004 Sumatra–Andaman earthquake, *Science,* 2005, vol. 308, pp. 1133–1139.

Araki, E., Shinohara, M., Obana, K., Yamada, T., Kaneda, Y., Kanazawa, T., and Suyehiro, K., Aftershock distribution of the 26 December 2004 Sumatra–Andaman earthquake from ocean bottom seismographic observation, *Earth Planets Space,* 2006, vol. 58, pp. 113–119.
https://doi.org/10.1186/BF03353367

Aron, F., Allmendinger, R.W., Cembrano, J., González, G., and Yáñez G., Permanent fore-arc extension and seismic segmentation: insights from the 2010 Maule earthquake, Chile, *J. Geophys. Res.: Solid Earth,* 2013, vol. 118, pp. 724–739.
https://doi.org/10.1029/2012JB009339

Azuma, R., Hino, R., Ohta, Y., Ito, Y., Mochizuki, K., Uehira, K., Murai, Y., Sato, T., Takanami, T., Shinohara, M., and Kanazawa, T., Along-arc heterogeneity of the seismic structure around a large coseismic shallow slip area of the 2011 Tohoku-oki earthquake: 2-D V_p structural estimation through an air gun-ocean bottom seismometer experiment in the Japan Trench subduction zone, *J. Geophys. Res.: Solid Earth,* 2018, vol. 123, pp. 5249–5264.
https://doi.org/10.1029/ 2017JB015361

Banerjee, P., Pollitz, F., Nagarajan, B., and Burgmann, R., Coseismic slip distribution of the 26 December 2004 Sumatra–Andaman and 28 March 2005 Nias earthquakes from GPS static offsets, *Bull. Seismol. Soc. Am.,* 2007, vol. 97, no. 1, part A, pp. 86–102.
https://doi.org/10.1785/0120050609

Barrientos, S.E. and Ward, S.N., The 1960 Chile earthquake: Inversion for slip distribution from surface deformation, *Geophys. J. Int.,* 1990, vol. 103, no. 3, pp. 589–598.
https://doi.org/10.1111/j.1365-246X.1990.tb05673.x

Ben-Menahem, A., The force system of the Chilean earthquake of 1960 May 22, *Geophys. J. R. Astron. Soc.,* 1971, vol. 25, pp. 407–417.

Beroza, G.C. and Ide, S., Slow earthquakes and nonvolcanic tremor, *Annu. Rev. Earth Planet. Sci.,* 2011, vol. 39, pp. 271–296.
https://doi.org/10.1146/annurev-earth-040809-152531

Bilek, S.L. and Lay, T., Rigidity variations with depth along the interplate megathrust faults in subduction zones, *Science,* 1999, vol. 400, pp. 443–446.

Campos, J., Hatzfeld, D., Madariaga, R., Lopez, G., Kausel, E., Zollo, A., Iannacone, G., Fromm, R., Barrientos, S., and Lyon-Caen, H., A seismological study of the 1835 seismic gap in South-Central Chile, *Phys. Earth Planet. Inter.,* 2002, vol. 132, pp. 177–195.

Chlieh, M., Avouac J.-Ph., Hjorleifsdottir V., Song, T.-R.A., Ji, Ch., Sieh, K., Sladen, A., Hebert, H., Prawirodirdjo, L., Bock, Y., and Galetzka, J., Coseismic slip and afterslip of the great M_w 9.15 Sumatra–Andaman

earthquake of 2004, *Bull. Seismol. Soc. Am.,* 2007, vol. 97, no. 1A, pp. 152–S173.
https://doi.org/10.1785/0120050631

Contreras-Reyes, E., Flueh, E.R., and Grevemeyer, I., Tectonic control on sediment accretion and subduction off south central Chile: Implication for coseismic rupture processes of the 1960 and 2010 megathrust earthquakes, *Tectonics,* 2010, vol. 29, paper ID TC0618.
https://doi.org/10.1029/2010TC002734

Cubas, N., Avouac, J.P., Leroy, Y.M., and Pons, A., Low friction along the high slip patch of the 2011 M_w 9.0 Tohoku-Oki earthquake required from the wedge structure and extensional splay faults, *Geophys. Res. Lett.,* 2013, vol. 40, pp. 4231–4237.
https://doi.org/10.1002/grl.50682

Delouis, B., Nocquet, J., and Vallée, M., Slip distribution of the February 27, 2010 $M_w = 8.8$ Maule earthquake, Central Chile, from static and high-rate GPS, InSAR, and broadband teleseismic data, *Geophys. Res. Lett.,* 2010, vol. 37.
https://doi.org/10.1029/2010GL043899

Dewey, J.W., Choy, G., Presgrave, B., Sipkin, S., Tarr, A.C., Benz, H., Earle, P., and Wald, D., Seismicity associated with the Sumatra-Andaman Islands earthquake of 26 December 2004, *Bull. Seismol. Soc. Am.,* 2007, vol. 96, no. 1A, pp. 25–42.

Dziewonski, A.M., Chou, T.-A., and Woodhouse, J.H., Determination of earthquake source parameters from waveform data for studies of global and regional seismicity, *J. Geophys. Res.,* 1981, vol. 86, pp. 2825–2852.
https://doi.org/10.1029/JB086iB04p02825

Ekstrom, G., Nettles, M., and Dziewonski, A.M., The global CMT project 2004–2010: Centroid-moment tensors for 13,017 earthquakes, *Phys. Earth Planet. Inter.,* 2012, vol. 200–201, no. 1–9.
https://doi.org/10.1016/j.pepi.2012.04.002

Engdahl, E.R., Villasenor, A., DeShon, H.R., and Thurber, C.H., Teleseismic relocation and assessment of seismicity (1918–2005) in the region of the 2004 M_w 9.0 Sumatra–Andaman and 2005 M_w 8.6 Nias Island great earthquakes, *Bull. Seismol. Soc. Am.,* 2007, vol. 97, no. 1A, pp. S43–S61.
https://doi.org/10.1785/0120050614

Farías, M., Comte, D., Roecker, S., Carrizo, D., and Pardo, M., Crustal extensional faulting triggered by the 2010 Chilean earthquake: the Pichilemu seismic sequence, *Tectonics,* 2011, vol. 30, paper ID TC6010.
https://doi.org/10.1029/2011TC002888

Fedotov, S.A., On the seismic cycle, possibility of quantitative division into seismic regions, and long-term seismic forecasts, in *Seismicheskoe raionirovanie SSSR* (Division of the USSR into Seismic Regions), Moscow: Nauka, 1968, pp. 121–150.

Geospatial Information Authority of Japan. The 2011 off the Pacific coast of Tohoku Earthquake, Coseismic and postseismic slip distribution on the plate interface (preliminary result). 2011. http://www.gsi.go.jp/cais/topic 110315.2-index-e.html.

Guilbert, J., Vergoz, J., Schissele, E., Roueff, A., and Cansi, Y., Use of hydroacoustic and seismic arrays to observe rupture propagation and source extent of the $M_w = 9.0$ Sumatra earthquake, *Geophys. Res. Lett.,*

2005, vol. 32, p. L15310.
https://doi.org/10.1029/2005GL022966

Hao, J.L., Wang, W.M., and Yao, Z.X., Source process of the 2011 M_w 9.0 Tohoku Japan earthquake, *Sci. China: Earth Sci.,* 2011, vol. 54, pp. 1105−1109.
https://doi.org/10.1007/s11430-011-4241-y

Hayes, G.P., Bergman, E., Johnson, K.L., Benz, H.M., Brown, L., and Meltzer, A.S., Seismotectonic framework of the 2010 February 27 M_w = 8.8 Maule, Chile earthquake sequence, *Geophys. J. Int.,* 2013, vol. 195, pp. 1034−1051.
https://doi.org/10.1093/gji/ggt238

Holdahl, S.R. and Sauber, J., in *Shallow Subduction Zone: Seismic, Mechanics and Seismic Potential,* Dmowska, R. and Ekstrom, G., Eds., Basel: Birkhauser, 1994.

Hsu, Y.-J., Simons, M., Avouac, J.-P., Galetzka, J., Sieh, K., Chlieh, M., Natawidjaja, D., Prawirodirdjo, L., and Bock, Y., Frictional afterslip following the 2005 Nias-Simeulue earthquake, Sumatra, *Science,* 2006, vol. 312, no. 5782, pp. 1921−1926.

Ide, S., Variety and spatial heterogeneity of tectonic tremor worldwide, *J. Geophys. Res.,* 2012, vol. 117, paper ID B03302.
https://doi.org/10.1029/2011JB008840

Idehara, K., Yabe, S., and Ide, S., Regional and global variations in the temporal clustering of tectonic tremor activity, *Earth Planets Space,* 2014, vol. 66.
https://doi.org/10.1186/1880-5981-66-66

Ishii, M., Shearer, P.M., Houston, H., and Vidale, J.E., Extent, duration and speed of the 2004 Sumatra−Andaman earthquake imaged by the Hi-Net array, *Nature,* 2005, vol. 435, no. 7044, pp. 933−936.

Ito, A., Yamamoto, Y., Hino, R., Suetsugu, D., Sugioka, H., Nakano, M., Obana, K., Kazuo Nakahigashi, K., and Shinohara, M., Tomographic image of crust and upper mantle off the Boso Peninsula using data from an ocean-bottom seismograph array, *Earth Planets Space,* 2017, vol. 69, no. 118, pp. 1−10.
https://doi.org/10.1186/s40623-017-0703-6

Kagan, Y.Y. and Jackson, D.D., Seismic gap hypothesis: ten years after, *J. Geophys. Res.,* 1991, vol. 96, pp. 21419−21431.

Kanamori, H., The Alaska earthquake of 1964: radiation of long-period surface waves and source mechanism, *J. Geophys. Res.,* 1970, vol. 75, pp. 5011−5027.

Kanamori, H. and Cipar, J.J., Focal process of the great Chilean earthquake, May 22, 1960, *Phys. Earth Planet. Inter.,* 1974, vol. 9, no. 2, pp. 128−136.
https://doi.org/10.1016/0031-9201(74)90029-6

Khazaradze, G., Wang, K., Klotz, J., Hu, Y., and He, J., Prolonged post-seismic deformation of the 1960 great Chile earthquake and implications for mantle rheology, *Geophys. Res. Lett.,* 2002, vol. 29, no. 22, p. 2050.
https://doi.org/10.1029/2002GL015986

Kiser, E. and Ishii, M., The March 11, 2011 Tohoku-oki earthquake and cascading failure of the plate interface, *Geophys. Res. Lett.,* 2012, vol. 39, paper ID L00G25.
https://doi.org/10.1029/2012GL051170

Koper, K.D., Hutko, A.R., Lay, T., and Sufri, O., Imaging short-period seismic radiation from the 27 February 2010 Chile (M_w 8.8) earthquake by back-projection of *P, PP,* and *PKIKP* waves, *J. Geophys. Res.,* 2012, vol. 117,

paper ID B02308.
https://doi.org/10.1029/2011JB008576

Kruger, F. and Ohrnberger, M., Tracking the rupture of the M_w = 9.3 Sumatra earthquake over 1150 km at teleseismic distance, Nature, 2005, vol. 435, pp. 937−939.

Lange, D., Tilmann, F., Barrientos, S.E., Contreras-Reyes, E., Methe, P., Moreno, M., Heit, B., Agurto, H., Bernard, P., Vilotte, J.-P., and Beck, S., Aftershock seismicity of the 27 February 2010 M_w 8.8 Maule earthquake rupture zone, *Earth Planet. Sci. Lett.,* 2012, vol. 317−318, pp. 413−425.

Lay, T., Kanamori, H., Ammon, Ch.J., Nettles, M., Ward, S.N., Aster, R.C., Beck, S.L., Bilek, S.L., Brudzinski, M.R., Butler, R., DeShon, H.R., Ekstrom, G., Satake, K., and Sipkin, S., The great Sumatra−Andaman earthquake of 26 December 2004, *Science,* 2005, vol. 308, pp. 1127−1133.

Lay, T., Ammon, C.J., Kanamori, H., Koper, K.D., Sufri, O., and Hutko, A.R., Teleseismic inversion for rupture process of the 27 February 2010 Chile (M_w 8.8) earthquake, *Geophys. Res. Lett.,* 2010, vol. 37, pp. 1−5.

Lay, T., Ammon, C.J., Kanamori, H., Xue, L. and Kim, M.J., Possible large near-trench slip during the 2011 M_w 9.0 off the Pacific coast of Tohoku Earthquake, *Earth Planets Space,* 2011, vol. 63, pp. 687−692.

Lay, T. and Kanamori, K., Insights from the great 2011 Japan earthquake, *Phys. Today,* 2011, vol. 64, pp. 33−39.

Lay, T., Kanamori, H., Ammon, Ch.J., Koper, K.D., Hutko, A.R., Ye, L., Yue, H., and Rushing, T. M., Depth-varying rupture properties of subduction zone megathrust faults, *J. Geophys. Res.,* 2012, vol. 117, paper ID B04311.

Lee, Sh.-J., Huang, B.-Sh., Ando, M., Chiu, H.-Ch., and Wang, J.-H., Evidence of large scale repeating slip during the 2011 Tohoku-Oki earthquake, *Geophys. Res. Lett.,* 2011, vol. 38, paper ID L19306.
https://doi.org/10.1029/2011GL049580

Lin, Y.-N.N., Sladen, A., Ortega-Culaciati, F., Simons, M., Avouac, J.-Ph., Fielding, E.J., Brooks, B.A., Bevis, M., Genrich, J., Rietbrock, A., Vigny, Ch., Smalley, R., and Socquet, A., Coseismic and postseismic slip associated with the 2010 Maule earthquake, Chile: Characterizing the Arauco peninsula barrier effect, *J. Geophys. Res.: Solid Earth,* 2013, vol. 118, pp. 3142−3159.
https://doi.org/10.1002/jgrb.50207

Lomax, A., Rapid estimation of rupture extent for large earthquakes: application to the 2004, M = 9 Sumatra−Andaman mega-thrust, *Geophys. Res. Lett.,* 2005, vol. 32, no. 10, paper ID L10314.

Lorito, S., Romano, F., Atzori, S., Tong, X., Avallone, A., McCloskey, J., Cocco, M., Boschi, E., and Piatanesi, A., Limited overlap between the seismic gap and coseismic slip of the great 2010 Chile earthquake, *Nat. Geosci.,* 2011, vol. 4, no. 3, pp. 173−177.

Lukk, A.A., Deshcherevskii, A.V., Sidorin, A.Ya., and Sidorin, I.A., *Variatsii geofizicheskikh polei kak proyavlenie determinirovannogo khaosa vo fraktal'noi srede* (Variations in Geophysical Fields as the Manifestation of Deterministic Chaos in a Fractal Medium), Moscow: OIFZ RAN, 1996.

Lukk, A.A. and Leonova, V.G., Focal mechanisms statistics in spatiotemporal vicinity of the 2011 Tohoku catastrophic earthquake, Japan, *Izv., Phys. Solid Earth,*

2020, vol. 66, pp. 169–188.
https://doi.org/10.31857/S0002333720020052

Lukk, A.A. and Leonova, V.G., Variations of kinematics of deformation in the vicinity of catastrophic Sumatran earthquake, *Geofiz. Prots. Biosfera,* 2018, vol. 17, no. 4, pp. 76–91.
https://doi.org/10.21455/GPB2018.4-5

Lyubushin, A.A., Cyclic properties of seismic noise and the problem of predictability of the strongest earthquakes in Japanese Islands, *Izv., Atmos. Oceanic Phys.,* 2018, vol. 54, no. 10, pp. 1460–1469.
https://doi.org/10.1134/S0001433818100067

McCann, W.R., Nishenko, S.P., Sykes, L.R., and Krause, J., Seismic gaps and plate tectonics: seismic potential for major boundaries, *Pure Appl. Geophys.,* 1979, vol. 117, pp. 1082–1147.

Melnick, D., Bookhagen, B., Strecker, M.R., and Echtler, H.P., Segmentation of megathrust rupture zones from fore-arc deformation patterns over hundreds to millions of years, Arauco peninsula, Chile, *J. Geophys. Res.,* 2009, vol. 114, paper ID B01407.
https://doi.org/10.1029/2008JB005788

Melnick, D., Moreno, M., Motagh, M., Cisternas, M., and Wesson, R.L., Splay fault slip during the M_w 8.8 2010 Maule, Chile, earthquake, *Geology,* 2012, vol. 40, no. 3, pp. 251–254.
https://doi.org/10.1130/G32712.1

Mogi, K., *Earthquake Prediction* (Tokyo: Academic Press, 1985; Moscow: Mir, 1988).

Mogi, K., Two kinds of seismic gaps, *Pure Appl. Geophys.,* 1979, vol. 117, no. 6, pp. 1170–1186.

Moreno, M.S., Bolte, J., Klotz, J., and Melnick, D., Impact of megathrust geometry on inversion of coseismic slip from geodetic data: application to the 1960 Chile earthquake, *Geophys. Res. Lett.,* 2009, vol. 36, p. L16310.
https://doi.org/10.1029/2009GL039276

Moreno, M., Rosenau, M., and Oncken, O., Maule earthquake slip correlates with pre-seismic locking of Aandean subduction zone, *Nature,* 2010, vol. 467, no. 7312, pp. 198–202.
https://doi.org/10.1038/nature09349

Moreno, M., Melnick, D., Rosenau, M., Bolte, J., Klotz, J., Echtler, H., Baez, J., Bataille, K., Chen, J., Bevis, M., Hase, H., and Oncken, O., Heterogeneous plate locking in the South-Central Chile subduction zone: building up the next great earthquake, *Earth Planet. Sci. Lett.,* 2011, vol. 305, nos. 3–4, pp. 413–424.

Natawidjaja, D.H., Sieh, K., Ward, S.N., Cheng, H., Edwards, R.L., Galetzka, J., and Suwargadi, B.W., Paleogeodetic records of seismic and aseismic subduction from Central Sumatra microatolls, Indonesia, *J. Geophys. Res.,* 2004, vol. 109, p. B04306.
https://doi.org/10.1029/2003JB002398

Nersesov, I.L., Ponomarev, V.S., and Teitel'baum, Yu.M., Effect of seismic quiescence before large earthquakes, in *Issledovaniya po fizike zemletryasenii* (Research in Earthquake Physics), Moscow: Nauka, 1976, pp. 149–169.

Nersesov, I.L. and Rulev, B.G., Dynamics of the development of long-term seismological precursors, *Izv. Akad. Nauk SSSR. Fiz. Zemli,* 1986, no. 1, pp. 39–51.

Ni, S., Kanamori, H., and Helmberger, D., Energy radiation from the Sumatra earthquake, *Nature,* 2005, vol. 434, p. 582.

Oleskevich, D.A., Hyndman, R.D., and Wang, K., The up-dip and downdip limit to great subduction earthquakes: Thermal and structural models of Cascadia, South Alaska, SW Japan and Chile, *J. Geophys. Res.,* 1999, vol. 104, pp. 14965–14991.

Ozawa, S., Nishimura, T., Suito, H., Kobayashi, T., Tobita, M., and Imakiire, T., Coseismic and postseismic slip of the 2011 magnitude-nine Tohoku-Oki earthquake, *Nature,* 2011, vol. 475, pp. 373–376.
https://doi.org/10.1038/nature10227

Ozawa, S., Nishimura, T., Munekane, H., Suito, H., Kobayashi, T., Tobita, M., and Imakiire, T., Preceding, coseismic and postseismic slips of the 2011 Tohoku earthquake, Japan, *J. Geophys. Res.,* 2012, vol. 117, paper ID B07404.
https://doi.org/10.1029/2011JB009120

Parkin, E.J., *Horizontal Crustal Movements Determined from Surveys after the Alaskan Earthquake of 1964, the Prince William Sound, Alaska, Earthquake of 1964 and Aftershocks,* Washington, D.C: U.S. Dept. of Comm. Coast and Geodetic Survey, 1969, vol. III.

Plafker, G., *Tectonics of the March 27, 1964 Alaska Earthquake. U.S. Geol. Surv. Prof. Paper.* 543–I, New York: U.S. Geol. Surv., 1969. https://pubs.usgs.gov/pp/0543i/.

Pollitz, F.F., Brooks, B., Tong, X., Bevis, M.G., Foster, J.H., Burgmann, R., Smalley, R.J., Vigny, C., Socquet, A., Ruegg, J.-C., Campos, J., Barrientos, S., Parra, H., Baez Soto, J.-C., Pritchard, M.E., and Simons, M., An aseismic slip pulse in northern Chile and along-strike variations in seismogenic behavior, *J. Geophys. Res.,* 2006, vol. 111, no. B8, paper ID B08405.
https://doi.org/10.1029/2006JB004258

Rebetskii, Yu.L., Development of the method of cataclastic analysis of shear fractures for tectonic stress estimation. *Dokl., Earth Sci.,* 2003, vol. 388, no. 1, pp. 72–76.

Rebetskii, Yu.L. and Marinin, A.B., Stressed state of the Earth's crust in the western region of the Sunda subduction zone before the Sumatra–Andaman earthquake on December 26, 2004, *Dokl. Earth Sci.,* 2006, vol. 407, no. 2, pp. 321–325.

Rebetsky, Yu.L. and Polets, A.Yu., The state of stresses of the lithosphere in Japan before the catastrophic Tohoku earthquake of 11 March 2011, *Geodyn. Tectonophys.,* 2014, vol. 5, no. 2, pp. 469–506.
https://doi.org/10.5800/GT-2014-5-2-0137

Ruegg, J.C., Rudloff, A., Vigny, C., Madariaga, R., de Chabalier, J.B., Campos, J., Kausel, E., Barrientos, S., and Dimitrov, D., Interseismic strain accumulation measured by GPS in the seismic gap between Constitución and Concepción in Chile, *Phys. Earth Planet. Inter.,* 2009, vol. 175, nos. 1–2, p. 78.
https://doi.org/10.1016/j.pepi.2008.02.015

Ruff, L. and Kanamori, H., Seismicity and the subduction process, *Phys. Earth Planet. Inter.,* 1980, vol. 23, pp. 240–252.

Scalera, G., Geodynamics of the Wadati–Benioff zone earthquakes: The 2004 Sumatra earthquake and other great earthquakes, *Geophys. Int.,* 2006, vol. 46, no. 1, pp. 19–50.

Scholz, C.H., Earthquakes and friction laws, *Nature,* 1998, vol. 391, pp. 37−42.

Shao, G., Li, X., Ji, Ch., and Maeda, T., Focal mechanism and slip history of the 2011 M_w = 9.1 off the Pacific coast of Tohoku earthquake, constrained with teleseismic body and surface waves, *Earth Planets Space,* 2011, vol. 63, pp. 559−564.
https://doi.org/10.5047/eps.2011.06.028

Shearer, P. and Bungmann, R., Lessons learned from the 2004 Sumatra−Andaman megathrust rupture, *Annu. Rev. Earth Planet. Sci.,* 2010, vol. 38, pp. 103−131.
https://doi.org/10.1146/annurev-earth-040809-152537

Sibuet, J.C., Rangin, C., Le Pichon, X., Singh, S., Cattaneo, A., Graindorge, D., Klingelhoefer, F., Lin, J.-Y., Malod, J., and Maury, T., 26th December 2004 great Sumatra−Andaman earthquake: Co-seismic and postseismic motions in northern Sumatra, *Earth Planet Sci Lett.,* 2007, vol. 263, no. 1−2, pp. 88−103.
https://doi.org/10.1016/j.epsl.2007.09.005.insu-00204272

Simoes, M., Avouac, J.P., Cattin, R., and Henry, P., The Sumatra subduction zone: a case for a locked fault zone extending into the mantle, *J. Geophys. Res.,* 2004, vol. 109, paper ID B10402.
https://doi.org/10.1029/2003JB002958

Simons, M., Minson, S.E., Sladen, A., Ortega, F., Jiang, J., Owen, S.E., Meng, L., Ampuero, J.-P., Wei, Sh., Chu, R., Helmberger, D.V., Kanamori, H., Hetland, E., Moore, A.W., and Webb, F.H., The 2011 magnitude 9.0 Tohoku-Oki earthquake: Mosaicing the megathrust from seconds to centuries, *Science,* 2011.
https://doi.org/10.1126/science.1206731

Subarya, C., Chlieh, M., Prawirodirdjo, L., Avouac, J.-Ph., Bock, Y., Sieh, K., Meltzner, A.J., Natawidjaja, D.H., and McCaffrey, R., Plate-boundary deformation associated with the Great Sumatra−Andaman earthquake, *Nature,* 2006, vol. 440, no. 7080, pp. 46−51.

Tajima, F., Mori, J., and Kennett, B.L.N., A review of the 2011 Tohoku-Oki earthquake (M_w 9.0): Large-scale rupture across heterogeneous plate coupling, *Tectonophysics,* 2013, vol. 586, pp. 15−34.

Tong, X., Sandwell, D., Luttrell, K., Brooks, B., Bevis, M., Shimada, M., Foster, J., Smalley, R., Jr., Parra, H., Soto, J.C.B., Blanco, M., Kendrick, E., Genrich, J., and Caccamise, D.J., II, The 2010 Maule, Chile, earthquake: downdip rupture limit revealed by space geodesy, *Geophys. Res. Lett.,* 2010, vol. 37.
https://doi.org/10.1029/2010GL045805

Trubitsyn, V.P., Model of the 2011 Japan earthquake (M = 9.0), *Geofiz. Prots. Biosfera,* 2011, vol. 10, no. 3, pp. 5−19.

Tsuru, T., Park, J., Takahashi, N., Kodaira, Sh., Kido, Y., Kaneda, Y., and Kono, Y., Tectonic features of Japan Trench convergent margin off Sanriku, northeastern Japan, revealed by multichannel seismic reflection data, *J. Geophys. Res.,* 2000, vol. 105, no. B7, pp. 16403−16413.
https://doi.org/10.1029/2000JB900132

Tsuru, T., Park, J., Miura, S., Kodaira, S., Kido, Y., and Hayashi, T., Along-arc structural variation of the plate boundary at the Japan Trench margin: Implication of interplate coupling, *J. Geophys. Res.,* 2002, vol. 107, no. B12, p. 2357.
https://doi.org/10.1029/2001JB001664

Vigny, C., Simons, W.J.F., Abu, S., Bamphenyu, R., Satirapod, Ch., Choosakul, N., Subarya, C., Socquet, A., Omar, K., Abidin, H.Z., and Ambrosius, B.A.C., Insight into the 2004 Sumatra−Andaman earthquake from GPS measurements in Southeast Asia, *Nature,* 2005, vol. 436, no. 7048, pp. 201−206.
https://doi.org/10.1038/nature03937

Vigny, C., Socquet, A., Peyrat, S., et al., The 2010 M_w 8.8 Maule megathrust earthquake of Central Chile, monitored by GPS, *Science,* 2011, vol. 332, pp. 1417−1421.
https://doi.org/10.1126/science.1204132

Wang, L., Shum, C.K., Simons, F.J., Tapley, B., and Dai, Ch., Coseismic and postseismic deformation of the 2011 Tohoku-Oki earthquake constrained by GRACE gravimetry, *Geophys. Res. Lett.,* 2012, vol. 39, paper ID L07301.
https://doi.org/10.1029/2012GL051104

Wang, K., Sun, T., Brown, L., Hino, R., Tomita, F., Kido, M., Iinuma, T., Kodaira, Sh., and Fujiwara, T., Learning from crustal deformation associated with the M9 2011Tohoku-oki earthquake, *Geosphere,* 2018, vol. 14, no. 2, pp. 552−571.
https://doi.org/10.1130/GESO 1531.1

Wells, D.L. and Coppersmith, K.J., New empirical relationships among magnitude, rupture length, rupture width, rupture area, and surface displacement, *Bull. Seismol. Soc. Am.,* 1994, vol. 84, pp. 974−1002.

Xu, Y., Koper, K.D., Sufri, O., Zhu, L., and Hutko, A.R., Rupture imaging of the M_w = 7.9 12 May 2008 Wenchuan earthquake from back projection of teleseismic *P*-waves, *Geochem., Geophys., Geosyst.,* 2009, vol. 10, p. Q04006.
https://doi.org/10.1029/2008GC002335

Yamamoto, Y., Obana, K., Kodaira, S., Hino, R., and Shinohara, M., Structural heterogeneities around the megathrust zone of the 2011 Tohoku earthquake from tomographic inversion of onshore and offshore seismic observations, *J. Geophys. Res.: Solid Earth,* 2014, vol. 119, pp. 1165−1180.
https://doi.org/10.1002/2013JB010582

Yamanaka, Y. and Kikuchi, M., Asperity map along the subduction zone in northeastern Japan inferred from regional seismic data, *J. Geophys. Res.,* 2004, vol. 109, paper ID B07307.
https://doi.org/10.1029/2003JB002683

Yunga, S.L., *Metody i rezul'taty izucheniya seismotektonicheskikh deformatsii* (Methods and Results of the Study of Seismotectonic Deformations), Moscow: Nauka, 1990.

Zhang, Y., Xu, L., and Chen, Y.-T., Rupture process of the 2011 Tohoku earthquake from the joint inversion of teleseismic and GPS data, *Earthquake Sci.,* 2012, vol. 25, pp. 129−135.
https://doi.org/10.1007/s11589-012-0839-1

Zhao, D., Huang, Z., Umino, N., Hasegawa, A., and Kanamori, H., Structural heterogeneity in the megathrust zone and mechanism of the 2011 Tohoku-oki earthquake (M_w 9.0), *Geophys. Res. Lett.,* 2011, vol. 38, paper ID L17308.

Translated by L. Mukhortova